AALBORG UNIVERSITY

MASTER THESIS IN MATERIALS TECHNOLOGY

---

# Sustainable carbon fibres from Lignin

---

| ***Authors:*** | ***Supervisor:*** |
|---|---|
| Alan Davis | Lars R. Jensen |
| Juhan Luik | |

The Faculty of Engineering and Science
Department of Materials and Production

15th of June 2021

AALBORG UNIVERSITY
STUDENT REPORT

AALBORG UNIVERSITY
STUDENT REPORT

**10th Semester**
**Engineering and Science**
Materials Technology
Fibigerstræde 16
9220 Aalborg East

**Title:**

Sustainable carbon fibres from Lignin

**Project:**

Master Thesis

**Project period:**

February 2021 - June 2021

**Members:**

Alan Davis
Juhan Luik

**Supervisor:**

Lars R. Jensen

**Number of pages: 64**
**Appendices: 2**
**Ended 15-06-2021**

**Abstract:**

The goal of this thesis was to create environmentally friendly carbon fibres with lignin as the precursor via the electrospinning method. They were activated to investigate them as a potential carbon capture material. Four of the tested solutions were able to produce uniform and unbeaded fibres, which were stabilised and carbonised without being fused together. The fibres were characterised and analysed with scanning electron microscopy, x-ray diffraction, Raman spectroscopy and their $CO_2$ adsorption was investigated in a thermogravimetric analyzer. The effects of the solution concentrations on the characteristics of the fibres were investigated, and carbon fibres with a diameter as low as 310 nm were produced. The Raman data showed similar results for all samples. The activated fibres were able to capture 28 mg/g of $CO_2$, which shows that this sustainable material has a potential in this application.

# Preface

This 10th semester Master thesis project was written by the undersigned authors as part of their Master's degree in Materials Technology at the Department of Materials and Production at Aalborg University. References to literature are made according to the IEEE citation style. Equations are abbreviated as Eq. (#) and are numbered according to their respective chapter and section.

## Acknowledgements

The authors wish to thank their supervisor Lars Rosgaard Jensen, for guidance with the theoretical and experimental parts of this project.
The authors also wish to thank Kim H. Jensen for help with the heat treatments, Thomas S. Quaade for help with the thermal analysis and Peter Kjær Kristensen for help with the SEM imaging, Donghong Yu for help with the XRD and Magnus Undell-Behrend Daugaard for introducing us to the electrospinning equipment.

Alan Davis Juhan Luik

# List of Abbreviations

| | |
|---|---|
| **KL** | Kraft Lignin |
| **PEO** | Polyethylene Oxide |
| **DSC** | Differential Scanning Calorimetry |
| **TGA** | Thermogravimetric Analysis |
| **CF** | Carbon fibres |
| **CNF** | Carbon nanofibres |
| **DMSO** | Dimethyl sulfoxide |
| **DMF** | Dimethyl formamide |
| **ACF** | Activated Carbon Fibre |
| **G** | Guaiacyl |
| **S** | Syringyl |
| **H** | P-hydroxyphenyl |
| **TSA** | Temperature swing adsorption |
| **PSA** | Pressure swing adsorption |
| **VSA** | Vacuum swing adsorption |
| **PAN** | Polyacrylonitrile |
| **XRD** | X-ray diffraction |

# Contents

# Chapter 1

# Introduction

The increase in green house gas emissions and other environmental impacts resulting from the use of petroleum based fuels and materials have made the development of renewable resource based alternatives a top priority. Natural polymers or biopolymers are widely available and are an alternative to petroleum based polymers, yet their potential is not fully utilised.

Lignin is the second most abundant natural polymer [1] and accounts for approximately 30% of the organic carbon that exists in the biosphere [2]. It is considered as the main aromatic renewable resource, with large quantities of it being produced as a byproduct of the paper and biomass fractionation industries [3]. With a worldwide production of 100 megatonnes per year [4], 98% of it is burned up and used for energy recovery. Lignin is yet to be converted into a high value product on a large scale as less than 2% of it being used for producing speciality chemicals such as dispersants, adhesives, surfactants and other value added products [5]. Lignin contains $60 - 66\%$ carbon and shows great potential in being utilised as a precursor for carbon fibres (CF)[6–11]. Traditionally, polyacrylonitrile (PAN) which is a petroleum based polymer is used to produce CF and replacing this with biopolymers such as lignin is highly beneficial[12].

Carbon dioxide contributes to three fourth of all green house gases produced and has impacted the environment by increasing global temperatures, triggering the melting of glaciers, rising of sea levels and acidification of oceans[13]. Carbon based absorbents are the most versatile absorbents for carbon dioxide. Utilising lignin based CF for absorption of carbon dioxide will not only reduce, but also offset the environmental impact from the paper and biorefinery industries.

The focus of the project is to develop carbon fibres from sustainable and environmentally friendly materials, such as lignin as the main precursor material and water as the solvent. The secondary objective is to produce fibres that have a small diameter, as that increases the specific area, which is a desirable quality for many applications. This can be achieved by creating carbon fibres with the electrospinning method. Finding processing parameters for the production of such fibres is the main goal of this project. The created lignin fibres will also be carbonised and activated to enhance their capability of capturing $CO_2$ from the atmosphere.

# Chapter 2

# Theory

The theory section will first discuss the materials used in this project, followed by a comprehensive overview of the electrospinning process and how the various parameters influence the outcome. Then there will be a short overview of the stabilisation and carbonisation processes, which are required to create carbon fibres. That will be followed by a short overview of different activation processes. The theory section will be concluded by an overview of possible applications for the produced fibres.

## 2.1 Lignin

Wood and plants are lignocellulosic materials which are mainly composed of cellulose, hemicellulose and lignin. Lignin is present mostly in the cell wall of these materials and strngthens them by binding the cellulose and hemicellulose structures. Lignin is a complex, highly branched, amorphous macro-molecule, with its structure, composition and molecular weight dependent on the plant source and extraction process [14]. The structure of lignin can be rationalised as a polymerised product of three basic phenylpropane monomers, also known as monolignols. These three monolignols are coniferyl, sinapyl, and p-coumaryl alcohols and are termed as guaiacyl (G), syringyl (S) and p-hydroxyphenyl (H) respectively inside the lignin structure (Fig. 2.1) [1].

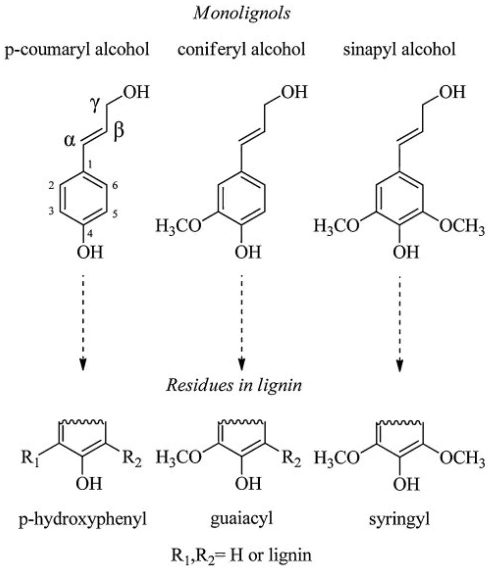

Figure 2.1: The structures of the three monolignols present in lignin polymers. Reproduced from [3] under the terms of Creative Commons CC BY license.

As the structure and properties of lignin vary with multiple factors such as plant species, location, extraction method, environment, etc., they can be mainly classified according to the biomass origin or the extraction method. Based on the biomass species it is classified as softwood, hardwood and non-woody lignin [15]. Softwood lignin is known to comprise of mostly G units with low levels of H units, while hardwood lignin comprises of G and S units with traces of H units. Whereas, non-woody lignin contain a mixture of all three units. [16] In order to better utilise lignin for value added materials, it has to be effectively isolated from lignocellulosics, and its physiochemical features and composition greatly depend on the extraction process [17]. Based on the extraction process lignin can be classified as Kraft lignin (KL), lignosulphonates, organosolv lignin, soda lignin, hydrolysis lignin and steam exploded lignin [18]. The molecular weight of lignin varies greatly based on the extraction method. The polydispersity of lignin is high for KL and lignosulphonates when compared to other types of lignin[1]. However, being an abundant source of renewable carbon with an aromatic structure, presence of phenolic and aliphatic groups, thermal stability and ease of availability makes it a potential candidate for carbon fibres[19].

### Kraft Lignin

Kraft pulping method is the mostly widely used method for converting wood to pulp and contributes to approximately 85% of the worldwide lignin production [14]. Kraft lignin is obtained in the form of a by-product known as black liquor. The kraft process is performed at high temperatures (~ 170° C) and high pH values (~ 13 – 14) where the lignin is dissolved in alkaline solutions of sodium hydroxide (NaOH) and sodium sulphide ($Na_2S$) making the solution turn dark brown [20]. In this process, the lignin macro-molecules get fractured, subsequently decreasing its molecular weight to 1 kDa to 5 kDa[1]. KL is soluble in aqueous alkaline solutions (pH $>$ 10.5) and in organic solvents such as dimethyl sulfoxide (DMSO) and dimethylformamide (DMF) due to creation of additional free phenolic groups by cleavage of aryl ether bonds during the Kraft process [21]. KL also contains a small amount of sulfur (<3%) as the nucleophilic attack of hydrosulphide ions on lignin retains some thiol groups[22] and can be removed with proper chemical treatment [23].

Researches have been able to produce lignin based carbon fibres of two types: single components fibres where lignin is the only precursor and multi-component fibres where lignin is blended with other polymers.

## 2.2 Binder Polymer

A binder polymer is generally added to lignin for the production of carbon fibres in order to provide the necessary chain entanglement required to produce continuous fibres. Some of the most commonly used binder polymers are polyacrylonitrile, polyvinyl alcohol and polyethylene oxide (PEO). Since the goal of our study is to produce environment friendly carbon fibres, PEO was chosen as the binder polymer.

### Polyethylene Oxide

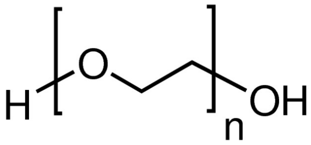

FIGURE 2.2: The structures of PEO

Polyethylene Oxide (PEO) is a linear polymer that can be produced with high molecular weights. Fig. 2.2 shows the structure of PEO and has the repeating unit of ethylene oxide ($-CH_2CH_2O-$) which contains a hydrophobic ethylene group and hydrophilic oxygen, which is also a hydrogen bond site[24]. However, PEO is generally hydrophilic in nature and is soluble in both water and polar solvents. Due to the nontoxic and nonimmunogenic properties, it is a heavily researched polymer in various biomedical applications.

## 2.3 Fibre production methods

Different fibre production methods were analysed, however as the goal was to make fibres for applications which require high specific surface areas, the focus was on the methods that are able to produce carbon nanofibres(CNF).

CNFs can be produced mainly by five different methods: catalytic chemical vapour deposition, electrospinning, templating, melt spinning or drawing[25]. This report focuses on the production of CNFs via the electrospinning method, because it has some important advantages compared to the other methods.

Chemical vapour deposition allows the creation of fibres with diameters down to 5 nm, however the produced fibres are relatively short, they are difficult to align, assemble and process for their ultimate application. It is also an expensive method with a low yield and a significant amount of residue.[25, 26]

Templating has the disadvantage of not being able to create continuous nanofibres and is not a scalable process[25]. The drawing method is a common process for creating carbon fibres in the micrometer range, however it is unsuitable for the creation of fibres in the nanometer range[27].

Melt spinning is another method for creating carbon fibres, although it does not allow the production of nanoscale fibres and the processing times can be prohibitively long for large scale production[27].

Electrospinning is a method that offers reasonably high yields, creates continuous fibres with a low diameter in the nanometer and easier processability. It also allows the production of both fibre mats and aligned fibres depending on the setup. It does not require expensive equipment and does not create waste products.[25]

## 2.4 Electrospinning

Electrospinning is the method of creating continuous fibres from a polymer solution or a melt. It is able to spin fibres with diameters in the nanometer range. The working principle of electrospinning is to use a high voltage in the kilovolt(kV) range to create an electrostatic force on the spinning solution, which is often in the form of a small droplet at the tip of a small orifice[28]. This electrostatic force deforms the droplet into a conical shape, which is called a Taylor cone, and out of the tip of the cone a jet of solution is accelerated towards the grounded collector, where the spun material gets deposited.

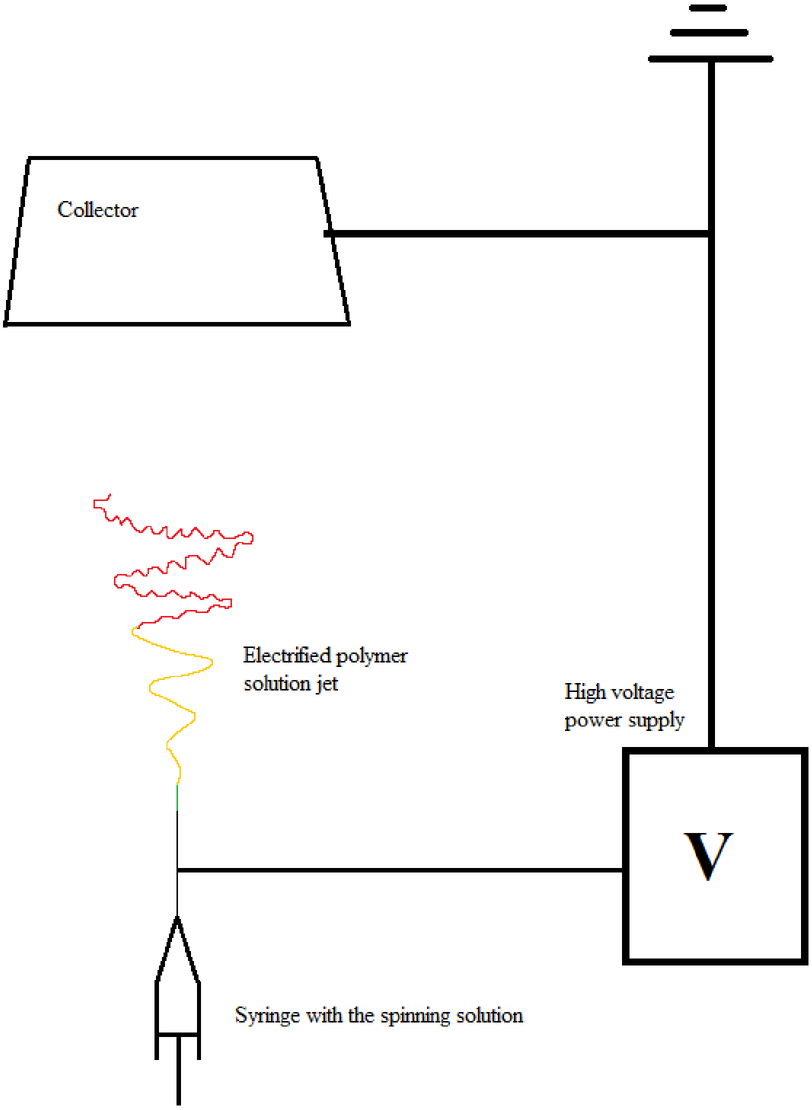

Figure 2.3: A schematic diagram of an electrospinning setup

In Fig. 2.3 a schematic of a simple electrospinning setup is shown. At the bottom there is a syringe filled with the spinning solution, which is pumped out of the needle at a controlled feed rate. The needle is connected to the high voltage power supply to apply the desired electric field to the solution. The applied voltage also charges the solution. As like charges repel each other, the excess charge in the droplet at the tip of the needle will be subjected to an electrostatic force trying to create separation between the charges. At the same time, surface tension is the force that is trying to keep the droplet intact. At a critical voltage, the electrostatic force will be equal to the surface tension and a Taylor cone will form. Increasing the voltage further, the electrostatic repulsion will overcome the surface tension and the solution will be accelerated towards the collector.[29, 30]

On the way to the collector, the solution will take the form of a jet if it is viscous enough or the form of droplets if it is not viscous enough. In the case of a continuous jet, fibres are created. Many factors affect how the jet acts during the flight from the tip of the needle to the collector. These will also determine the morphology of the resulting fibres and are vital to understand. The jet starts off as a straight jet towards the collector(marked green in Fig. 2.3), becoming thinner over the distance due to the stretching of the jet and the evaporation of the solvent. The jet does not stay straight for long, as the repulsive electrostatic forces create a bending instability. This instability is due to the repulsive electrostatic interactions between nearby charges in the polymer jet. This instability makes the jet spiral and take a longer path to the collector, which results in the jet having more time to stretch, more time for the solvent to evaporate and will result in thinner fibres. In Fig. 2.3 the yellow segment of the jet shows the first bending instability, where the jet starts spiralling around the axis of the straight segment. The red segment shows the second bending instability, where the jet starts spiralling around the axis of the first spiral. Higher level bending instabilities also occur, with each next one spiralling around the axis of the previous level instability.[29–31]

The jet also experiences Rayleigh instability, which is caused by the surface tension trying to minimize the surface area of the liquid. Rayleigh instability tries to break the jet into droplets, as droplets have a lower specific surface area than a jet. This can result in the jet breaking up into droplets or the resulting fibres containing beads. This will be discussed in more detail in Section 2.4.

As the jet gets thinner over the path to the collector, another instability appears due to the modulation of the surface charge density. This can result in the fibres containing beads[32].

At the top, a flat collector plate can be seen in Fig. 2.3, which is also connected to the electrical circuit with the power supply. At the collector the fibres are deposited and depending on the parameters used, they can take the form of uniform fibres, fibres with a flat ribbon like cross-section or porous fibres.

The morphology of the fibres depends on the processing parameters used, which can be categorised into three main categories. First there are the solution parameters, which include viscosity, conductivity, surface tension and the volatility of the solvent. Then there are the spinning setup parameters, which include the applied voltage, the tip-to-collector distance, the solution feed rate, the needle size and the collector type. And finally, there are the ambient parameters, which are the relative humidity and the temperature. Each of these play an important role in determining the properties of the resulting fibres. There are also practical considerations for the setup, like the needle orientation and the collector type, which might not have a big impact on the morphology of the fibres, but that might influence otherwise the quality of the mat or the ease of processing. Next we will take a closer look into each of the parameters and how they influence the morphology of the fibres.

### Electrospinning Parameters

This section will give an overview of the parameters that need to be considered for the production of electrospun fibres. The solution parameters will be summarized first, followed by the spinning setup parameters and finally the ambient parameters will be discussed.

### Surface Tension

Surface tension is a phenomenon caused by the molecules at the surface of the solution not having molecules on all sides. This pulls the surface molecules inward and creates an inward force that tries to reduce the total surface area of the solution.

Overcoming the surface tension of the droplet at the tip of the needle is a necessary condition for electrospinning. Therefore, the required critical voltage to initiate and conduct electrospinning depends on the surface tension of the spinning solution and a solution with a higher surface tension requires a higher minimal applied voltage to be spun.

Apart from affecting the initiation of the jet, surface tension also affects the shape of the jet during the flight from the needle to the collector, as it will continue to try to reduce the overall area of the jet. During the flow of a liquid, the surface tension will cause the liquid to break up into droplets, which is a phenomenon called Rayleigh instability. However, to break the jet up or even create beads, the Rayleigh instability needs to overcome two forces. First, there is the viscosity of the solution, which limits the mobility of the molecules in the solution to aggregate into beads. And secondly in electrospinning there is the surface charge, which is stretching the jet and working against the formation of beads. [33, 34]

If the viscosity of the solution is low, there are more free solvent molecules in the jet and as the solvent molecules are much more mobile than the polymer molecules, they tend to aggregate and form beads. A study by Fong et al. looked at the effect of surface tension on bead formation by using a mixture of ethanol and water as the solvent and varying the ratio of ethanol to water[33]. Their results showed that higher surface tension due to the increased water content increases the formation of beads.

Surface tension is a parameter that affects the choice of solvent for an electrospinning solution. If the surface tension is too high, the required applied voltage to conduct electrospinning becomes very high, which has its own consequences discussed in more detail in Section 2.4, and it also increases the chance of the fibres containing beads or making the spinning impossible due to the breakup of the jet.

### Conductivity

Electrospinning uses electrostatics to accelerate the solution from the needle to the collector and to make this possible, the solution has to contain charges. Thus, the solution has to conduct the charges from the needle to the solution and therefore its conductivity influences the process significantly. The conductivity will define the charge density within the polymer jet, as higher conductivity will allow more charge to flow through the same volume of solution.

A high enough charge density is required to break the surface tension of the solution droplet at the tip of the needle, and that is helped by a higher conductivity. The charge density also influences how much the solution gets stretched before arriving at the collector, with higher charge density causing the jet to be stretched more and the resulting fibres having smaller diameters[35, 36].

Angammana and Jayaram analyzed the effects of the solution conductivity on the fibre morphology by adding NaCl to the solution and found that an increased conductivity resulted in lower fibre diameter[35].

The second effect of increased conductivity and the resulting higher charge density is that it increases the force that the surface tension must overcome to create beaded fibres[37].

However, at higher conductivities the formation of multiple jets can happen, which is caused by the enhancement of the local electric field at the surface of the fluid due to the higher concentration of ions[35].

Increasing the conductivity does not decrease the diameter of the fibres linearly. Above a certain value of conductivity the electrostatic forces stretch the jet too much and if nothing else is changed, the jet will become discontinuous. One simple way to counter a too high charge density is to increase the feed rate of the solution. However, increasing the feed rate has the effect of making the fibres thicker. The combined effect of increasing the conductivity and feed rate can result in either an increase or decrease of the fibre diameter, depending on which effect dominates.[38, 39]

### Viscosity

Viscosity is another key parameter of the solution during electrospinning. Viscosity of the polymer solutions comes from the friction between the entangled, swollen polymer molecules and the solvent molecules surrounding them, but also depends on the chosen solvent[30]. A better solvent that is able to dissolve the polymer more easily will increase the viscosity as the interactions between the solvent molecules and the polymer molecules are stronger[30]. It is a key reason why the jet does not break up during the path from the needle to the collector due to Rayleigh instability. In a solution with a high viscosity, the solvent molecules interact with the polymer chains significantly, and are well distributed along the polymer chains without aggregation.[30]

The effect of viscosity has been studied extensively by different authors. Fong et al. looked at the effect of viscosity on bead formation by spinning aqueous PEO solutions of different concentrations. They found that higher viscosity reduced the occurrence of beads in the fibres. As the viscosity increased, the beads started occurring less frequently and at a specific viscosity uniform fibres were formed.[33]

Authors have looked at the morphology of Lignin&PEO solutions in DMF and found that the fibre diameter increases with an increase in viscosity. As the electrostatic forces try to stretch the solution, viscosity is what opposes this stretching. The shear stress in the jet is constant if the jet diameter is assumed to be constant, which means that as the viscosity increases, the shear rate decreases. As the shear rate is the amount of stretching, the increase in viscosity increases the diameter of the fibres. It also reduces the bending instability of the jet, which results in a shorter path from the needle to the collector, giving the fibre less opportunity to stretch. A lower bending instability also narrows the area where the fibres are deposited, as the jet does not bend as much and will not deviate from the shortest distance to the collector. [7–9, 30]

Multiple authors also report that highly viscous solutions become impossible to spin if they exceed a certain viscosity value, due to the solution drying out at the tip of the needle[37, 40].

Solution viscosity depends on a few parameters. An increase in the polymer concentration will increase the viscosity of the solution. Secondly, an increase in the molecular weight of the polymer also increases the viscosity. The strength of the interaction between the solvent and the polymer molecules also plays a minor role in the viscosity of the solution.[30]

In more complex setups, there can be more constituents in the electrospinning solution, that is, the solvent might consist of multiple species or there could be a mix of polymers and/or solvents or there could be additives in the solution to optimise other solution properties. In general, the same principles apply if only one variable is changed. However, when combining two polymers in a solution, they can generate complexes[6]. Due to the formation of complexes, the increase in viscosity as a result of adding more of one component is not linear any more. Each species has a limited capability of creating complexes, which means that the viscosity of the solution increases with one function within some range and when no more complexes can be made, the viscosity of the solution increases with a different function.

Dallmeyer et al. investigated the effects of lignin and PEO concentration changes on the solution viscosity. In their results, if the lignin to PEO ratio remained constant, then increasing the overall polymer content increased the viscosity. They also increased the PEO concentration at different lignin concentrations. At a lignin concentration of 25 % the addition of just 0.1 % of PEO increased the viscosity by 25 % from 19 mPa · s to 24 mPa · s and the addition of another 0.1 % increased it to 28 mPa · s, however at a lignin concentration of 45 % the addition of 0.1 % of PEO increased the viscosity from 1598 mPa · s to 2023 mPa · s. The increase is similar, however when the PEO concentration was increased to 0.2 %, the viscosity rose only to 2082 mPa · s. While the addition of 0.1 % of PEO still increased the viscosity about 25 %, the addition of another 0.1 % increased it very minimally. This suggests that within that solution system the addition of PEO of 0.1 % has a big influence on the viscosity of the solution, however adding more lignin increases the viscosity only marginally.[10]

Poursorkhabi et al. compared the viscosity of PEO&lignin mixture solutions in different solvents and reported that the solvent has a big effect on the viscosity. When using water as a solvent for an 11 % overall polymer content solution, the viscosity was about 0.45 Pa · s, while the same polymer mix in DMF had a viscosity of about 0.08 Pa · s.[6]

They also looked at the effect of storage time on the solution viscosity by measuring the viscosity 2-3 hours and 24 hours after the solutions were mixed. Their results show a significant decrease in viscosity of about 50 % to 80 %. This can be explained by the relaxation of the PEO molecules in the solution state over time. It can take up to 24 hours for the PEO solution to reach equilibrium. The relaxation of the PEO molecules reduces the number of entanglements and in the case of PEO/lignin complexes reduces the elasticity of the solution.[6]

### Evaporation of the solvent

Evaporation of the solvent is another necessary condition for getting electrospun fibres. During the path from the needle to the collector, the jet must dry out and become a solid fibre. This requires the solvent to evaporate or else no individual fibres will be produced. It could result in the fibres being fused together or the deposition of a film of the polymer solution if evaporation barely takes place.[30]

The evaporation rate of a solvent depends on multiple factors - the vapour pressure, the boiling point, the humidity, the specific heat, the enthalpy and heat of vaporisation of the solvent, the ambient temperature, the interaction between the solvent molecules and between the solvent and solute molecules, the surface tension and the air movement around the liquid surface[30]. The solvent evaporates more easily if it has a high vapour pressure, a low boiling point, low surface tension or if it does not have strong interactions with the solute[41].

The effect of the solvent evaporating too fast has negative consequences as well, as it becomes difficult to initiate electrospinning. Jarusawannapoom et al. used 18 different solvents for spinning polystyrene, and some of the more volatile solvents were unspinnable at higher polymer concentrations[40]. They attributed the drying out of the solution at the tip of the needle to the solvent evaporating too fast and making the solution unspinnable.

Liu et al. investigated different solvent systems for polystyrene fibres. By using solvents with different evaporation rates, they were able to create fibres with different morphologies. If the evaporation rate is different enough, then it becomes possible to create porous or grooved fibres. They propose two mechanisms for grooved fibres. The first one suggests that the highly volatile solvent evaporates and creates a glassy skin and voids on the surface of the fibre due to fast evaporation and phase separation and the less volatile solvent keeps the fibre 'wet' and stretchable, which allows the stretching of the voids into grooves. The second mechanism proposed is similar to the first, with the difference being that instead of voids, the fast evaporation creates wrinkles on the surface of the fibre.[42]

Celebioglu and Uyal found that it is possible to create porous fibres by combining two volatile solvents. The mechanism described suggests that porous fibres are created when one of the solvents evaporates faster and creates a local phase separation. The areas where the more volatile species is in abundance and evaporate faster will lead to creation of pores. The polymer will dry and solidify after the evaporation and the result will be a porous fibre.[43]

The choice of solvent has significant effects on both the spinnability of the solution and the morphology of the resulting fibres. By choosing the appropriate solvent, the fibres can be made uniform, ribbon-like, porous or grooved.

### Voltage

The application of a voltage to the needle and the creation of a potential difference between the needle and the collector is the basis of the electrospinning method, and deciding how big that potential difference should be is another key parameter in the process. Applying a potential charges the solution and creates a force to shape the solution into a fibre.

The applied voltage creates a few effects which drive the process. Firstly, it charges the solution and, the charged particles strongly repel each other due to electrostatics thereby forcing them to the surface of the solution. In the droplet at the tip of the needle, this surface charge will be counteracted by the surface tension. If the applied voltage is high enough, the electrostatic forces will equal the surface tension and the solution will take the shape of a cone, which is referred to as the Taylor cone[44, 45].

If the strength of the electrostatic force exceeds the surface tension, then a jet will be ejected from the cone towards the collector. At voltages just above the critical voltage needed to create a jet, it is still unlikely to be a stable jet. To achieve a stable jet, the voltage needs to be somewhat higher than the critical voltage[37]. Zong et al. found that the critical voltage for poly(d,l-lactic acid) in DMF was 16 kV, but a stable cone and an uninterrupted jet was only achieved above 20 kV[37].

An increase of the voltage also increases the charge density within the jet, which leads to a stronger force stretching the jet during the path from the needle to the collector[46]. Increasing the voltage a lot above the critical voltage also draws more mass out of the needle. This can result in the Taylor cone moving inside the needle unless the feed rate is increased. If the feed rate is increased, the fibre diameter increases due to the initial jet diameter being larger[47]. If the cone moves inside the needle, the fibres start containing beads due to the change in the shape from which the jet originates from[37].

The second effect of the applied voltage is a creation of an electric field between the needle and the collector. This electric field increases the acceleration of the polymer solution from the tip of the cone towards the collector. As the jet gets stretched throughout the path to the collector, it is advantageous to try to keep the voltage lower to increase the time when the jet can get stretched to obtain thinner fibres.[30, 46]

When solutions with low viscosities are spun with a high applied voltage, then multiple jets can occur. The jets repel each other as they are charged and distribute themselves over a larger area on the collector compared to just one jet. [48]

Wu et al. looked at the influence of different charging systems and found that if the collector is being charged and the needle is being grounded, the fibre diameters are about 20 % smaller. They found that it significantly influences the distance over which the jet takes a straight path. The straight jet distance was over 11 mm whenthe needle was charged at various voltages and between 3 mm to 6 mm when the collector was charged. They also reported a significantly higher angle for the whipping instability for the solutions when the collector was charged, suggesting that the decrease in the fibre diameter is due to the extra stretching that comes from the longer path to the collector. They also made an experiment with an electropositive charger, which was used to charge both the needle and the collector, but this did not improve the fibre morphology.[49]

### Solution feed rate

The feed rate of the solution governs the quantity of the solution that needs to be carried away from the tip of the needle to the collector by the applied voltage. As discussed in Section 2.4 about applied voltage, the amount of solution that gets accelerated towards the collector depends on the applied voltage. Therefore, the solution feed rate is tied to the applied voltage in the sense that the goal of adjusting those two parameters is to create a stable jet that creates continuous fibres.

The effect of the feed rate on the fibre diameter is not entirely clear. Some authors have shown that it does not significantly influence the morphology of the fibres[50–52], while others have shown that an increase in feed rate increases the diameter of the fibres[37, 53]. Tan et al. spun different concentration solutions of poly(l-lactic acid) and found that the average fibre diameter does not change[50]. Kong et al. spun corn starch and created a model describing how different parameters influence the diameter of the fibres, and reported that adding a term for the feed rate to their model does not improve the fit[51]. Beachley and Wen spun polycaprolactone and found that the feed rate does not have an influence on the diameter over their parameter variations and that it only increases the amount of polymer that is suspended at the tip of the needle[52].

However, Zong et al. spun poly(d,l-lactic acid) and poly(l-lactic acid) and found that increasing the feed rate created thicker fibres and beads as the thicker jet will not be able to dry out before reaching the collector[37]. Wang et al. also spun poly(d,l-lactic acid) and showed that the diameter of the fibres increases from 498 nm to 804 nm if the feed rate is increased from 1 ml/h to 4 ml/h[53]. They also analyzed the effect of feed rate on the height of the straight part of the jet and concluded that a higher feed rate increases the length of the straight part of the jet and that the electric field at the end of the straight jet gets smaller. This causes the whipping instability to be less efficient at prolonging the path to the collector and results in thicker fibres[53].

The difference between these studies seems to be that the ones that reported the difference in the fibre diameters with varying feed rates have looked at the diameters of fibres that have beads, while the papers that show the fibre diameter being independent of the feed rate only look at uniform fibres.

An appropriate feeding rate has to be chosen, as very low feed rates can lead to jet initiation inside the needle, which makes them unstable, and very high feed rates can lead to collection of excess material at the needle tip resulting in electrospray.[54]. Electrospray can happen when there is too much material at the tip of the needle, as the applied voltage will not be able to create a sufficient amount of charge in the jet and stretch such an amount of material. This will result in the solution still being accelerated onto the collector, but without being stretched. The presence of such excess material also affects the rest of the mat by introducing solvent to the mat, which can fuse the already spun fibres together.

### Needle

The needle diameter influences the flow of the material to the Taylor cone. At a constant feed rate, if a needle with a smaller diameter is used, the material flows out from the needle faster, but with the initial jet radius being smaller.

The needle diameter can also have an effect on the solution viscosity. If the solution is shear thinning, then a smaller diameter needle will increase the shear rate and thus reduce the viscosity. He et al. looked at the effect of the needle size on the spinning of PEO fibres and found that the needle diameter has an effect on the diameter of the fibres. They looked at seven different needle diameters and looked at the fibre diameters both with a constant flow rate and at a constant flow velocity through the needles. In both cases, the smaller diameter needles created thinner fibres. They explained that with the increase in viscosity due to the shear thinning effects.[55]

Liang et al. looked at the effect of the needle diameter to the spinning of poly(lactic acid) and found that smaller diameters create thinner fibres and also make them more porous[56].

Hekmati et al. looked at the influence of needle length on the fibre diameter. They found that using a shorter needle could be used to decrease the fibre diameter. They spun polyamide-6 fibres with needles ranging from 10 mm to 40 mm long. The fibre diameters of the 10 mm needle were 155 nm, while the others were between 255 nm to 286 nm. They hypothesize that the fibre diameter difference could come from the reduction of kinetic energy of the solution in the longer needles. They suggest that this reduces the amount of bending and whipping that the solution undergoes and therefore the fibres end up with a larger diameter.[57]

### The collector

As the collector acts as a ground to the applied voltage on the needle, the characteristics of the collector will have an influence on the fibres. Different materials and configurations can be used to manipulate how the fibres are collected. The collector choice determines, whether the fibres have random orientation or uniform orientation. Depending on the material used, it can also influence the deposition rate.

The simplest collector is a grounded metal plate, where the fibres are deposited in a random orientation over a specific area, the size of which depends on the other spinning parameters. Stanger et al. looked at the effect of different collector materials and found that if the material does not have a high enough conductivity, then the deposition rate will drop due to the substrate not being able to conduct the charge away and the incoming fibres being repelled by the existing charges.[58]

There are a few ways to achieve fibres that are better aligned. One of those ways is to introduce a gap between two collectors that are at the same distance. This results in the fibre collecting on both collectors, but as it switches between the two collectors, there will be fibres that are suspended in the gap between the two collectors. These fibres are reasonably well aligned. Liu et al. investigated the effects of such gaps and found that the orientation was not very good at gaps below 5 cm and that at distances above 5 cm the alignment improved, but not much.[59]

Li et al. spun poly(vinyl pyrrolidone) solutions onto a quartz substrate with conducting gold strips applied onto that substrate. They showed that aligned fibres can be created on insulators. The incoming fibres are affected by three electrostatic forces: the collector, the external field and adjacent charged fibres. On a metal plate collector the charge is carried away, and the fibres do not influence the alignment. But if an insulating gap is present, it changes the structure of the external electric field. The charged fibres will induce opposite charges on the electrodes, which will further attract the fibre to the electrodes. The collected fibres also repulse the incoming fibres, which directs the new fibres towards an alignment parallel to the collected fibres, as that is the more stable configuration.[60]

Li et al. also investigated making patterned fibre mats by having multiple gold strips that are positioned perpendicularly to each other. If four such strips are used and just two of them are grounded at a time, then it is possible to create layered fibre mats, where each layer consists of fibres aligned in a specific direction.[60]

Many more authors have used a rotating cylinder or a rolling drum to collect aligned fibres. The idea is to rotate the collector at high enough speeds that the fibres are pulled by the collector into the preferred alignment. De Prá et al. studied the effects of different rotating collectors on polycaprolactone fibres. They used a static drum, a drum with a diameter of 10 cm rotated at 2000 rpm and static parallel copper wires separated by 1 cm. With a static drum they reported fibres with a diameter of 1142 nm diameter and the rotating drum produced fibres with just 663 nm in diameter. While the static drum collected fibres in a random orientation, the rotating drum collected fibres, out of which more than 75 % were less than 20 degrees off, relative to the zero angle. The copper wires did align the fibres better than just the static drum, but as the mat grew thicker on this setup, the alignment of the fibres also became more random.[61]

With the rotating drum, the rotation speed is another variable that can be changed. At speeds that are lower than the fibre take-up speed, the fibres are not that well oriented. At too high speeds, the fibres stop being continuous. However, in between there is a range of speeds that give continuous aligned fibres as the rotating drum can also stretch them without breaking them up to a point.[62]

There are multiple collector types suggested in the literature and the choice will have an effect on the fibre alignment and deposition rate. Depending on the application the appropriate collector has to be chosen, because fibre alignment might be imperative for the desired properties and the deposition rates can differ significantly. However, it is hard to estimate the deposition rates due to papers rarely reporting them.

### Humidity

The ambient properties also have an effect on the outcomes of the electrospinning. The evaporation of the solvent depends on the vapour pressure and the vapour pressure is related to humidity via the saturated vapour pressure[63]:

$$p = \phi \cdot p_s \tag{2.1}$$

where $p$ is the vapour pressure, $\phi$ is the relative humidity and $p_s$ is the saturated vapour pressure. If the relative humidity is high, then the difference between the vapour pressure and the saturated vapour pressure is small, and the solvent does not evaporate as quickly, which will result in fibres with a larger diameter and possibly wet fibres on the collector that fuse together[63].

Tripatanasuwan et al. looked at the effect of humidity on the fibre diameter of a 6% PEO ($M_w$=400 000 $g/mol$) solution and found that increasing the humidity decreases the fibre diameter, however at a relative humidity of over 50% the fibres started including beads. Their experiment suggested that the humidity helped keep their solution to avoid solidification and continue to elongate. Due to a lot of elongation and the consequent drop in charge density, the fibre started getting beaded as the surface tension started to overcome the forces resisting beading. Above that humidity level, experiments at higher humidities created bigger beads with smaller distances between each bead.[64]

De Vrieze et al. studied the effect of humidity on poly(vinylpyrrolidone) solutions with 7 % and 10 % concentrations in ethanol. In their experiment, high relative humidity prohibits the creation of fibres due to the solution absorbing ambient water during spinning, which causes wet fibres and fusion on the collector. Within the limits of spinnability, the diameter of the fibres decreases with higher humidity due to the evaporation taking longer and keeping the fibres from solidifying significantly before reaching the collector.[65]

De Vrieze et al. also looked at the effect of humidity on cellulose acetate solutions in acetone:N,N-Dimethylacetamide and there the outcome was the opposite - a higher humidity resulted in fibres with a larger diameter. They suggest that this can be explained by the cellulose acetate precipitating out of the solution faster due to it being insoluble in water, which restricts the stretching of the jet. [65]

This suggests that the effect of humidity on the fibre diameter depends on the polymer species and the solubility of the species in water needs to be accounted for.

### Temperature

Temperature is another ambient variable that has an effect on the electrospinning outcomes. While it doesn't have a direct effect on the outcomes, it does affect important parameters like solution viscosity, surface tension, conductivity and evaporation rate.[66]

It is common knowledge that solution viscosity decreases at higher temperatures, however the chain entanglement is relatively independent of the solution temperature. This suggests that it is possible to find a minimal spinnable concentration and use a solution of that concentration at an elevated temperature to reduce viscosity and as a result the fibre diameter.[66]

Wang et al. found that the conductivity of PAN/DMF solutions increases with temperature, which increases the charge density of the jet and results in thinner fibres. They also found that the surface tension decreases with increased temperature. Mituppatham et al. on the other hand found that the conductivity of their polyamide-6 solution in formic acid decreased with an increased temperature.[39, 66]

The evaporation rate of the solvent plays a significant role as well at higher temperatures. De Vrieze et al. looked at the effect of temperature on poly(vinylpyrrolidone) solutions in ethanol and just by going to 30 °C the evaporation rate of the solvent was already so high that during the flight the jet dried out too quickly and the resulting fibre was thicker than the one that was spun at 20 °C.[65]

Electrospinning at elevated temperatures can improve the properties of the fibres created with specific solutions, but the properties of the constituents of the solution need to be looked at to understand whether increasing the temperature would also result in better fibres.

## 2.5 Stabilisation

Stabilisation is an important intermediate step in producing CNF as it prevents sticking, shrinking, or melting of the fibres during carbonisation. During this process, the fibres undergo multiple chemical reactions namely cyclization, dehydrogenation and oxidation with volatile byproducts being removed from them[67]. Consequently, the lignin changes from a thermoplastic to a thermoset material by rearranging its intermolecular atomic bonding patterns[68]. Various method such as oxidative, electron-beam irradiation, UV radiation and plasma treatment are used to stabilise CNFs. However, oxidative stabilisation is the most common method used for lignin based CNFs and is performed in an environment of air or oxygen.

When a polymer is heated at slow heating rates, the glass transition temperature ($T_g$) increases fast enough such that the polymer always remains in a glassy state[69]. This mechanism is used to increase the $T_g$ of the electrospun fibres so that carbonisation can be performed at very high temperatures. The three major phenomena that take place during stabilisation are heat transfer, mass transfer and shrinkage. The mass transfer involves diffusion of oxygen into the fibres and evolution of gases such as hydrogen. The shrinkage occurring during stabilisation can be chemical or physical, with the former occurring due to the chemical reactions taking place and the latter as a result of entropy recovery.[70]

The heating rate is an important parameter in the stabilisation process as the process is oxygen controlled and heating rates that favour maximum increase in oxygen content is desirable[71]. Low heating rates of $0.05 - 5°Cmin^{-1}$ are preferred for the effective oxidative stabilisation of fibres[72]. Several studies have shown that lower heating rates are favourable for stabilisation of lignin fibres, probably due to auto-oxidation[73]. It also increases the formation of cross-links in the structure, resulting in an increase in $T_g$. An improper heating rate can prevent the diffusion of oxygen to the inner structure, resulting in a skin-core structure which has an oxygen rich, compact structure on the outside and an oxygen deficit, less dense structure in the interior[74].

Another important factor that affects the stabilisation process is the temperature, as the oxygen content in the resulting fibre is temperature dependent[75]. Li et al. conducted a study on the oxygen content of KL stabilised at various temperatures $(170 - 350°C)$ and found that the oxygen content increases up to $260°C$ and reduces at higher temperatures.[76]

Applying tension on the precursor fibre during stabilisation also has an effect on the properties of the resulting CFs. It aids in reducing chain relaxation and maintaining a highly oriented structure, as it provides additional energy for the molecules to be packed into ordered phases[77, 78]. It is actively used to improve the mechanical properties (tensile strength and modulus) of CFs derived from various polymers[79–81].

## 2.6 Carbonisation

The final step in the production of CFs is the carbonisation process, which is performed in an inert atmosphere at higher heating rates to temperatures above $600°C$. During this process, non-carbon elements react and evaporate as by-products and a carbonised structure is formed[82]. The leads to a significant weight loss $(50 - 60wt\%)$[83] and reduction in diameter[84] of the resulting CFs. The parameters affecting the resulting CFs are heating rate, final holding temperature and carbonising medium[85]. The carbonisation is performed in an inert environment such as nitrogen or argon to prevent the oxidation of the fibres at such high temperatures and dilute the evolved gases[86].

The heating rate used in the carbonisation process is an important parameter as it affects the performance of the resulting carbon fibres[87]. A higher heating rate will introduce defects in the carbon fibre, while a lower heating rate can cause too much gasification (evolution of $\mathrm{N_2, CO_2 \,\&\, H_2O}$) in the early stages of the process, both of which are undesirable[72].

The temperature at which carbonisation is performed is also an important factor, with higher temperatures resulting in a higher degree of order in the carbon structure as reactions occurring during this process are completed at that specific temperature[88]. Increasing the carbonisation temperature also increases the tensile strength and elastic modulus of lignin based carbon fibres, achieving their highest values at $900°C$ and $1000°C$ respectively[89]. An increase in surface area, an increase in pore diameter, pore volume and an increase in crystallite size of the graphite sections of the resulting CF were also reported with an increase in carbonisation temperatures[85].

Another parameter that can improve the mechanical properties of the resulting CFs is the application of tension, as it reduces fibre shrinkage and increases molecular orientation[87][89].

## 2.7 Activation

Activated carbon fibres (ACFs) are CFs with highly porous structure and a large surface area ($500 - 2000 m^2 g^{-1}$). This property has led to its usage in a wide range of applications such as catalysis, filtration, deodorisation and decolourisation[90]. ACFs can be classified as microporous, mesoporous or macroporous depending on the pore diameter. They are produced by activating CFs by physical or chemical activation methods.

Physical activation is done right after the carbonisation process and is performed by introducing oxidising gases such as carbon dioxide or steam at an elevated temperature ($600 - 1200°C$)[91][92]. The gases react with the carbon, resulting in the removal of the more disorganised carbon and the formation of pores[93].

In chemical activation the stabilised fibres are first treated with a chemical activation agent such as hydroxides (NaOH or KOH) or acids (phosphoric, nitric or sulphuric acids) and carbonised and activated in the same step[94, 95]. Chemical activation often leads to higher pore volumes and wider pore sizes[93].

### Activation with carbon dioxide

CFs are held at high temperatures for hours with a steady flow of $CO_2$ in order to produce ACFs. They have shown to produce micropores with larger volume and narrower size distribution than those activated by steam[96].

$$\mathrm{C} + \mathrm{CO_2} \longrightarrow 2\,\mathrm{CO} \tag{2.2}$$

The $CO_2$ gas reacts with the carbon in the fibres and produces carbon monoxide during this process (Eq. (2.2)).

Schlee et al. activated lignin-based carbon fibres with $CO_2$ at 800 °C for one hour. They reported a yield of 75 % from the carbonised fibres and the pore volume doubling as a result of the activation[97]. They achieved specific surface area of about 350 $m^2/g$

Ra et al. activated PAN-based nanofibre paper with $CO_2$ for four hours at temperatures between 700 °C to 1000 °C. They found that higher temperatures increased the specific surface area more. The increase in specific surface area came mostly from the extra micropores(0.5 nm to 2 nm) and mesopores($>$2 nm) created while the surface area of the ultramicropores($<$0.7 nm to 0.8 nm) was reduced slightly. They achieved specific surface areas between 300 and 700 $m^2/g$.[98]

Choma et al. activated Kevlar-based carbon fibres with $CO_2$ at 700 °C to 800 °C for 0.5 h to 5 h. The higher temperatures and longer times increased the specific surface area, with a maximal area of 1240 $m^2/g$ achieved with an activation of 5 hours at 750 °C. They did not report anything for the sample activated for 5 hours at 800 °C, which based on the trends from the other experiments should give a very high specific surface area sample. The lack of reporting on this suggests that they were unable to create a sample with those parameters.[99]

Amaral et al. activated PAN-based carbon fibres with $CO_2$ at 1000 °C for 50 minutes and achieved a specific surface area of 1260 $m^2/g$[100].

## 2.8 Applications

Due to the ease of availability, low cost, reduced environmental impact and high carbon content of lignin, CFs derived from them have gained significant increase in scientific exploration. Lignin based CFs have been used as reinforcements, energy storage materials, electrodes in electrochemical applications, adsorbent and purification materials [101–104].

Lignin derived carbon materials are finding increased usage in electrochemical applications due to its high corrosion resistance, high specific area, porous structure, high electrical conductivity and low cost[101]. Babel et al. reported a high hydrogen electrosorption of 510mAh/g for KL derived activated carbon and, thus, showed promise for its use as a negative electrode in rechargeable hydride batteries[105]. Lignin derived CNF for electrochemical storage as supercapacitor cells has also been demonstrated. Hu et al. reported that ACFs produced from electrospun KL& PEO blends shows high gravimetric capacitance of 344 F/g and outstanding cycling stability, indicating its efficient use in supercapacitors with aqueous electrolytes[106]. Wang et al. reported high specific capacity of up to 445mAh/g at a current density of 30mA/g for fused CNF mats made from Lignin & PEO blends as an electrode in Li-ion batteries. These values are comparable to PAN derived CNFs and was further improved by nitrogen doping and thermal annealing in urea.[107] Jin et al. reported that CNF mats derived from hardwood lignosulfonate & PAN blends of equivalent ratios exhibited a reversible capacity of about 292.6 mAh/g, good rate capability and excellent cycling stability for application in Na-ion batteries[108].

Lignin based activated carbon is also utilised in applications for adsorption, with the major drawback being that the source of the lignin can heavily influence the properties of the activated carbon such as surface functionality, porosity and morphology[109].

Lignin based activated carbon has shown high adsorption of dyes such as methylene blue and methyl orange from aqueous solutions[110–112]. Toxic organic molecules such as phenolic compounds, endosulfan, sulfamethazine, ibuprofen, acetaminophen, BTX (benzene, toluene and xylene) and crude oil have also been studied for their adsorption properties with lignin derived activated carbons.[113–117]. With the increase in green house gas emissions, lignin derived activated carbons have also been researched on their adsorption properties of gases such as $CO_2, SO_2 \,\&\, H_2S$[118–120]. Another key area of research for lignin derived activated carbon is in adsorption of heavy metal ions such as lead (Pb), mercury (Hg), cadmium (Cd), chromium (Cr), arsenic (As), zinc (Zn), copper (Cu) and nickel (Ni) from water[121].

### CO2 adsorption

Activated carbon is viewed as an efficient material for adsorption of $CO_2$ due to their large surface area, wide availability, high, hydrophobicity, high thermal stability and good chemical resistance[122]. Depending on the configuration of the fossil fuel-based power plant, carbon dioxide partial pressure and gas stream pressure, carbon dioxide capture methods can be classified as pre-combustion, post-combustion and oxy-combustion carbon capture technologies[123].

In a pre-combustion process, the fuel (coal or natural gas) is pre-treated by gasification, where a synthesis gas, which is a mixture of carbon monoxide and hydrogen gas is formed[124]. However, this process is complex and requires a large upfront cost in retrofitting the plants[125]. In oxy-combustion process, the fuel is combusted in $O_2$ instead of air resulting in a flue gas that is enriched in $CO_2, H_2O$ and $SO_2$ which are separated with further processing[126]. This method has the advantage of low separation and capturing cost, with the major drawback being the high energy utilisation during the separation of $O_2$ from air[127]. Post-combustion process, $CO_2$ is captured and separated from the flue gas, which is produced after combustion of the fuel and is rich in $CO_2$ and $N_2$[128]. This method is currently the most widely adopted method due to its ease of retrofitting in existing plants, with the major drawback being the low concentration of $CO_2$ in the post combustion flue gas(4 %–14 %)[129].

For capturing $CO_2$ from the flue gases, several separation methods such as absorption, adsorption, membrane separation and cryogenics can be used[130]. In absorption, liquid sorbents such as diethanolamine, monoethanolamine and potassium carbonate which have a good adsorption capacity and a low regeneration energy are used[131]. However, its drawbacks are the high regeneration energy requirement, solvent degradation, production of volatile compounds and erosion of equipment[132]. The use of a semipermeable membranes (metallic, ceramic or polymeric) to separate $CO_2$ from the flue gas has achieved an efficiency of 82 %–88 %[133, 134]. But, the performance of these membranes are reduced with the low concentration and pressure of $CO_2$ and the presence of impurities in the flue gas[135]. In cryogenic distillation, the gas undergoes distillation at very low temperatures and very high pressure[136]. This method cannot be implemented for post-combustion methods due to the presence of large amounts of impurities and incondensable gases in the flue gas and also since refrigeration is an energy intensive process[123].

Adsorption is seen as one of the most promising technologies where a solid sorbent is used to bind the $CO_2$ molecules to its surface. A good adsorbent has a large specific area, high selectivity and high regeneration ability, with typical adsorbent materials being molecular sieves, activated carbon, zeolites, calcium oxides, hydrotalcites and lithium zirconate[136]. In this method, $CO_2$ is captured on the surface of the adsorbent by chemisorption, where the adsorbate is attached to the surface of the adsorbent via covalent bonding, or by physisorption, where the adsorbate gets attached to the surface of the adsorbent with the help of electrostatic and Van der Waals forces[137]. The cyclic adsorption of the adsorbate is done through three different regeneration processes: temperature swing adsorption (TSA), pressure swing adsorption (PSA) and vacuum swing adsorption (VSA)[138]. In PSA and VSA, the pressure inside the adsorbent fitted column is reduced, resulting in desorption of the gas. In both methods, the column is first filled with flue gas until saturation for adsorption, after which, the pressure is reduced to ambient pressure in PSA and to vacuum in VSA for desorption[139, 140]. In TSA, the adsorbent fitted column is filled with flue gas for adsorption and heated till the desorption temperature[141]. The use of waste or low grade thermal energy from the plant for the heating cycle makes this process economically viable and has been gaining more interest[142].

## Chapter 3

# Materials and Methodology

### Materials

Softwood kraft lignin (BioPiva$^{\mathrm{TM}}$395) with an average molecular weight of 6000 g mol$^{-1}$ was purchased from UPM Biochemicals (Finland).

PEO with an average molecular weight of $1,000,000$ g mol$^{-1}$ was purchased from Sigma Aldrich.

### Sample Preparation

The solution preparation consisted of two steps. Firstly, separate solutions of PEO in water and lignin in 0.5 M NaOH were made separately overnight at room temperature and mixed with a magnetic stirrer at a low speed. The next morning, the solutions were mixed in the desired ratios for 15 minutes with a magnetic stirrer. The solutions were kept at rest for an hour before electrospinning to get rid of any shear effects from mixing[6].

In Table 3.1 the contents of the studied solutions are presented.

Table 3.1: The constituents

| Solution | Lignin:PEO | Tot polymer | m(PEO)[g] | m(lignin)[g] | m(solution)[g] |
|---|---|---|---|---|---|
| A | 93:7 | 8 % | 0.20 | 2.66 | 35.71 |
| B | 95:5 | 8 % | 0.14 | 2.65 | 34.96 |
| C | 95:5 | 10 % | 0.28 | 5.31 | 55.94 |
| D | 97:3 | 10 % | 0.20 | 6.44 | 66.46 |
| E | 93:7 | 6% | 0.20 | 2.66 | 47.61 |
| F | 95:5 | 6% | 0.14 | 2.66 | 53.2 |

The electrospinning setup consisted of a high voltage power source(Glassman PS/MJ30P0400-22), which was connected to the needle and grounded to the collector.

Figure 3.1: The electrospinning setup used. The high voltage supply is just outside the picture on the bottom right, connected to the needle in the centre at the bottom of the picture. The collector is a folded aluminium foil that is attached to the steel plate, which is connected to the ground wire seen at the top left.

The needle was fixed to the bottom of the setup at a fixed height ( 5 cm) from the base. The collector, which was a steel plate with three holes, was fixed to the base using three long bolts. These bolts had nuts on which the collector was locked in. The distance from the needle tip to the collector could be changed by adjusting these nuts to the desired height on the bolts. The bolts had plastic jackets around them for insulation so that the fibres wouldn't collect on them. The collector used for the final experiments for collecting fibre mats was a folded aluminium foil, as pictured in Fig. 3.1. The collector with airgaps between five straight collectors was used to make it easier to collect the fibres from the collector for further processing. At small quantities it also allows the creation of aligned fibres, however at longer spinning times the alignment becomes random.

The whole setup was inside a fume hood with a safety switch that disconnected the circuit to the power supply when the fume hood was opened. Between the power source and the needle, there was a multimeter attached to the circuit that measured the voltage applied to the needle. The other part of the setup was a syringe pump, where a 20 ml syringe was attached. The syringe was attached to the needle by a 20 cm plastic tube of inner diameter 6 mm. There was an electronic thermometer and a hygrometer in the fume hood to monitor the ambient parameters.

The oven used was a Nabertherm R40/500/12 tube oven, which allowed heating rates up to about 50 °C per minute, but had no active cooling. It had an atmosphere control system with inlets for air, argon and $CO_2$ with controllable flow rates. It also had a dry scroll vacuum pump attached to allow for creating a pure atmosphere. The dimensions of the inner tube where the samples were put was 2.8 cm and the oven was able to maintain the desired temperature for 6 cm to 8 cm at the centre of the tube.

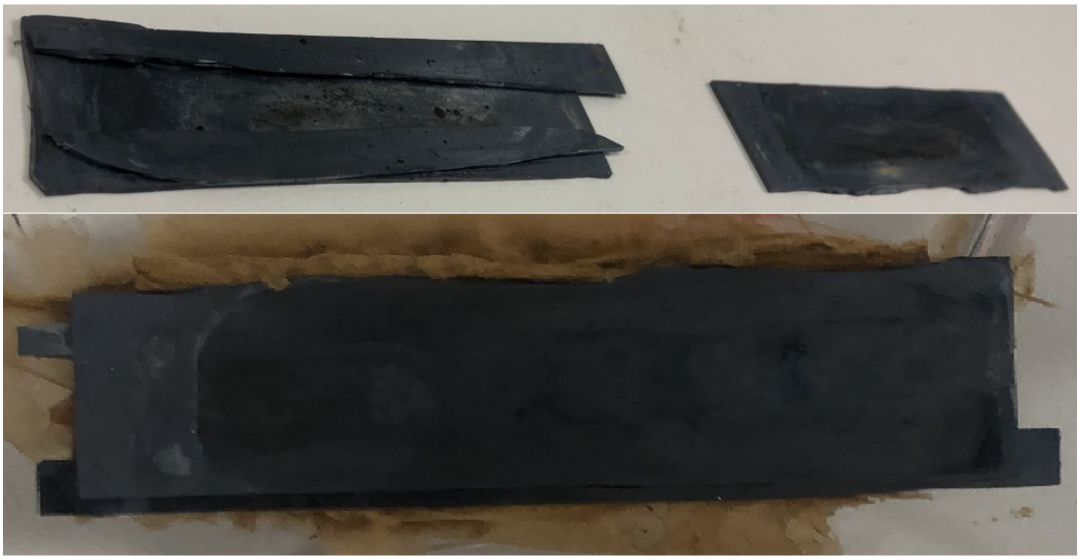

Figure 3.2: The fixture for keeping the fibre mats from shrinking. On the top image the bottom and the top of the fixture can be seen separately without any fibres and on the bottom image the fixture can be seen with fixed fibres.

To keep the samples fixed in the oven, silicon wafers and an alumina boat were used to fix the sample and prevent it from moving. A 6 cm by 2 cm silicon wafer piece was cut to be used as the base on top of which the electrospun fibre mat was placed. This fixture can be seen in Fig. 3.2. After placing the samples on it, two thin strips of Si wafers 3 mm by 6 cm were placed on top of the samples along the edges of the base wafer. That was to keep the fibres from contracting during the oven treatments. On top of these, another 6 cm by 2 cm silicon wafer was placed to make the setup more stable. An alumina boat with a weight of 28 g was placed on top of the wafers to make sure that the samples are kept in place.

Stabilisation was carried out at the temperature of 250 °C for one hour with a heating rate of 0.5 °C per minute and the samples were passively cooled overnight to room temperature. There was a constant flow of air through the oven of 100 ml/min throughout the whole process. The procedure was carried out at atmospheric pressure.

Carbonisation was carried out at the temperature of 1000 °C for one hour with a heating rate of 5 °C per minute. Throughout the process, a flow of Argon with a purity of 99.999 % at the rate of 75 ml/min was used. The oven was evacuated and purged with Argon thrice at the start of each experiment to purify the atmosphere of other gases. The procedure was carried out at atmospheric pressure. The samples were passively cooled in Argon atmosphere to room temperature.

Activation was carried out at the temperature of 800 °C for 15 minutes. The samples that were activated were not cooled down to room temperature after the carbonisation, but at 800 °C the oven was vacuumed and filled with $CO_2$ for 15 minutes with a flow of 100 ml/min. After that, the oven was vacuumed and purged with Argon and then filled with Argon to atmospheric pressure. After that, the normal cooling with an Argon flow of 75 ml/min was continued until the oven reached room temperature.

All solutions were spun at the tip to collector distance of 20 cm, temperature was 21 °C, the needle used was 20G, which has an inner diameter of 0.603 mm and the collector was as described above.

The rest of the electrospinning parameters were as follows:

Table 3.2: The spinning parameters for the electrospinning experiment. Column Tot polymer is referring to the total polymer content of the solution.

| Solution | Lignin:PEO | Tot polymer | Voltage | Feed rate | Humidity |
|---|---|---|---|---|---|
| A | 93:7 | 8 % | 21 kV | 0.15 ml/h | 39,7% |
| B | 95:5 | 8 % | 27 kV | 0.7 ml/h | 28,4% |
| C | 95:5 | 10 % | 21 kV | 0.3 ml/h | 29,1% |
| D | 97:3 | 10 % | 21 kV | 0.4 ml/h | 27,7% |
| E | 93:7 | 6% | 21 kV | 0.3 ml/h | 21,9% |

## Characterisation

Differential scanning calorimetric analysis (DSC) was carried out using TA DSC Q2000, samples of approximately 5 mg to 8 mg were scanned at a rate of 10°C/min from −60 °C to 250 °C under an inert atmosphere of $N_2$ gas. The first and second heating curves are reported.

Thermogravimetric analysis (TGA) was carried out using TA Discovery SDT650, samples of 8 mg were heated at a rate of 10°C/min from 25°C to 800°C under an inert atmosphere of $N_2$ gas.

The shear viscosity of the solution were measured using a TA AR-G2 rheometer with a cone and plate geometry with a cone diameter of 60 mm and angle of 0.995 833°. The truncation distance was 29 µm. Samples were loaded using a syringe with an average volume of 1 ml to fill the geometry gap. Flow sweep tests were conducted at 25 °C from a shear rate of 1.0 / sec to 100 / sec.

Fibre morphology was investigated with SEM Zeiss Evo 60. Sample preparation for carbon fibres was simply mounting them on the SEM stage on carbon tape. The fibres imaged just after spinning and after stabilisation were sputter coated with gold. The fibre diameters were analysed with ImageJ software. A representative image of the fibre mat was taken and imaged at a resolution where the diameter of at least 50 fibres could be measured.

Raman spectroscopy was done with a Renishaw Invia micro-Raman spectroscope and a 532 nm laser was used for irradiating the sample.The Raman spectra were recorded at five different positions on the carbonised fibre mat. The measurement was taken with a laser power of 5% and 30 scans of 1 sec were conducted to obtain the spectra. The resulting spectra was manually baseline corrected and peak fitted using the software Fityk. The graphitic mole fraction ($x_G$) and the crystallite size ($L_a$) were calculated using the below equations.

$$x_G = \frac{1}{1+R} \tag{3.1}$$

$$L_a = \left(2.4 \times 10^{-10}\right) \lambda^4 (R)^{-1} \tag{3.2}$$

where R is the ratio between the intensity of the D and G band ($R = I_D/I_G$) and $\lambda$ is the wavelength of the incident laser.

X-ray diffraction (XRD) patterns were collected with an Empyrean diffractometer (PANalytical) using Cu $K_\alpha$ radiation and a voltage and working current of 45 V and 40 mA, respectively. The measurement range of $2\theta$ was 5-55° with a step size of 0.00328°. The samples were crushed into powder using a mortar and pestle to conduct the measurement. The interlayer spacing ($d_{002}$) and the crystallite size ($L_a$) were calculated from the below equation.

$$d_{002} = \frac{\lambda}{2 \sin\theta} \tag{3.3}$$

$$L_\mathrm{a} = \frac{K\lambda}{B \cos\theta} \tag{3.4}$$

where $\lambda$ is the wavelength (1.5406Å), $\theta$ is the Bragg angle and $B$ is the full width at half maximum of the corresponding peaks. The value of $K$ is 0.89 for (002) peak.

### CO2 adsorption measurement

The $CO_2$ adsorption-desorption experiments were carried out using a TA Discovery TGA to precisely measure the mass gain or loss. The flow rate of all gases were 50ml/min. The samples of 2 mg were loaded onto an aluminium pan and initially degassed under an $N_2$ stream at 110°C for 120 min. The temperature was reduced to 25°C at a heating rate of 10°C/min and held for 60 min. $CO_2$ adsorption-desorption was analysed by changing the gas to $CO_2$ for 60 min and later switched to $N_2$ for 60 min.

# Chapter 4

# Preliminary Experiments

## 4.1 Solution Parameters

The preliminary experiments were necessary in this project as there was no literature that had used the same combination of materials. There are plenty of papers[7–11, 107] that have done experiments with DMF as the solvent, however there is only one that uses water as a solvent[6]. However, in that paper they used PEO of molecular weights 200 000 g/mol and 5 000 000 g/mol. They were unable to create fibres with any of the solutions that used the PEO with the lower molecular weight. As a result, it was important to determine the range of solution concentrations in terms of the overall content and the lignin:PEO ratio that can be electrospun.

The study by Poursorkhabi et al.[6] also used water as a solvent and looked at a range of 5 % to 11 % overall polymer content and Lignin:PEO weight ratios of 97:3 and 95:5. The preliminary experiments took that as a basis for choosing the solution parameters. While there are multiple parameters to consider, the starting point seemed to be to vary the lignin and PEO contents in the solution. Water was chosen as a solvent due to the environmentally friendly nature of the project, and it was chosen to keep the conductivity of the solution constant throughout the preliminary studies. That was to keep the amount of variables in the solution to a reasonable level so that it would be easier to make conclusions about the solution, should the experiments not yield desired results.

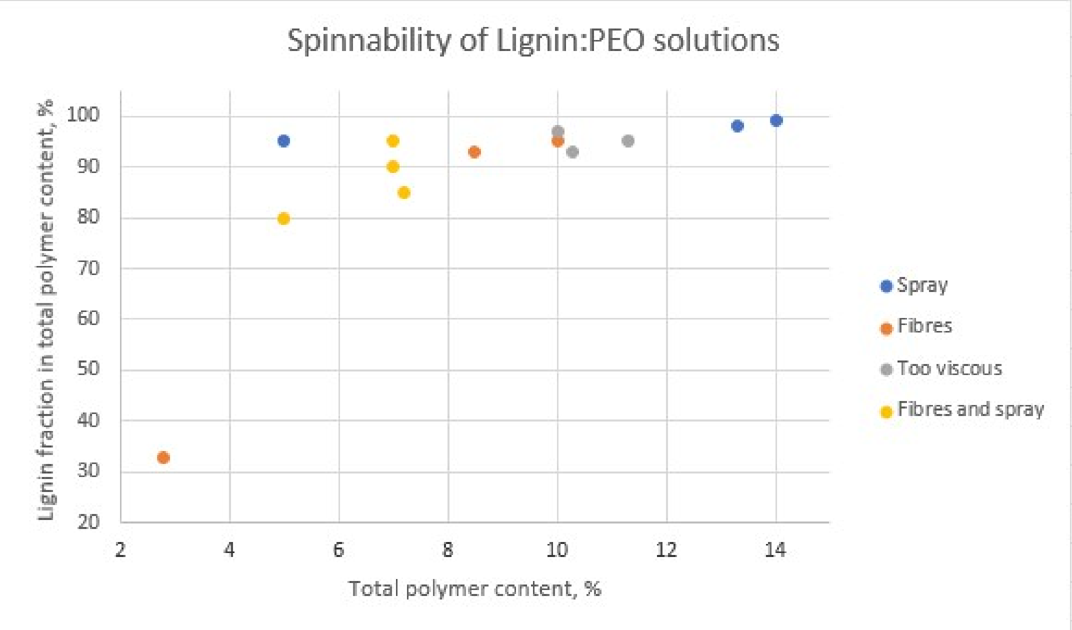

FIGURE 4.1: The spinnability of lignin:PEO solution

The solutions tested in the preliminary study are shown in Fig. 4.1. The full details with brief comments about the resulting fibres can be found in Appendix A. On the x-axis is the total polymer content, which is strongly dominated by the amount of lignin in the solution. On the y-axis is the lignin content as a fraction of the total polymer content. The dots represent the different solutions tested in the preliminary study. The goal of the preliminary experiment was to find out what range of lignin:PEO ratios and overall polymer contents can produce fibres by electrospinning. The other important consideration made when choosing the solution concentrations was to try to use the minimal amount of PEO. That was chosen as the goal of the project is to create carbon fibres from lignin and reduce the amount of PEO.

Lignin:PEO ratios ranging from 80:20 to 98:2 were tested. The conclusions of the preliminary study showed that any solution, where the lignin:PEO ratio was higher than 97:3 was not spinnable. The solutions did not have enough of the binder polymer of PEO to create fibres, and the outcome was that the solution was electrosprayed onto the collector. This was regardless of the amount of lignin, as the 98:2 solution mentioned in Fig. 4.1 had a high lignin content and high enough viscosity. The same outcome of electrospraying happened at a lignin:PEO ratio of 95:5 with a low overall polymer content of 5 %.

There were four samples tested with the lignin:PEO ratio of 95:5 at overall polymer contents of 5 %, 7 %, 10 % and 11.3 %. The sample with 11.3 % overall polymer content was too viscous to spin, the 10 % solution produced fibres, the 7 % solution gave a mix of fibres and electrospray. This line of solutions shows a range of overall polymer contents for a lignin:PEO ratio of 95:5, that is useful for spinning and also suggests that if the lignin:PEO ratio is higher than 95:5, then it is very unlikely that a solution with an overall polymer content of 7 % could be spinnable.

Another solution at 5 % total polymer content with the lignin:PEO ratio of 80:20 was done in the beginning, which produced some less than ideal fibres, which shows that the 5 % total polymer content is enough to create a solution with an appropriate viscosity.

The spinnability of the solutions was also looked at a lignin:PEO ratio of 93:7, where already an overall polymer content of 10.3 % created a solution that was too viscous to spin. This means that at a lower lignin:PEO ratio, the maximum overall polymer content that can be spun is lower. And secondly a comparison with two solutions with 10 % overall polymer content, but a higher lignin:PEO ratio showed that the region of concentrations within which fibres can be created is reasonably small.

However, even during the preliminary study, some complications were encountered that impacted the reproducibility of the spinning experiments. After a few spinnable solutions had been created, the syringe used in the experiment stopped functioning properly. It was unable to keep a constant feed rate at all times and instead sometimes slowed down the feed rate and then jumped and suddenly pushed a bigger amount of solution to the tip of the needle. It was not immediately evident that this might be because of the syringe, as this could be a property of a poorly spinnable solution as well.

The protocols for mixing the solutions in literature cited a mixing for two hours at 60 °C for the lignin:PEO solution in water while the polymers were added slowly[6]. However, in our case, this procedure did not fully dissolve the PEO. With the slow adding of PEO, it took about six hours to create a solution with a high enough PEO content for the experiment. It also required someone to regularly add the polymer as the viscoelastic properties of the solution change over time and would have not been feasible to create solutions like that. Different approaches were tried to make this part of the project less time consuming. Dissolving the PEO at higher temperatures was tried, however the resulting solutions had very low viscosity. This could be due to solution approaching the melting temperature of PEO or scission of PEO chains due to stirring at high temperatures. The eventual solution was to dissolve the PEO in water by adding the required amount at once and stirring it slowly overnight at room temperature.

The preliminary experiment thus suggested that fibres could be spun from solutions which have around 5 % to 10 % total polymer content and the lignin:PEO ratio of around 5 %. The result of the preliminary study is that it was decided to investigate total polymer contents of 6 %, 8 % and 10 % were chosen and the lignin:PEO ratios of 93:7, 95:5 and 97:3 in more detail.

## 4.2 Electrospinning Parameters

The electrospinning parameters for the different solutions were investigated as well from the perspective of finding out a range of parameters to use for the main experiment.

The electrospinning setup allowed the tip to collector distance, the voltage, the needle and the feed rate to be changed. It was not possible to control the humidity, which varied between relative humidity values of 17 % and 50 %, which was always recorded, but did not seem to have a significant effect on the spinnability. Temperature was monitored and was always 21 °C or ± 0.3 °C.

The voltage range of the setup was between 0 kV to 30 kV and the spinning distance could be anywhere up to 30 cm. However, as the legs holding the collector were about 15 cm from the needle, increasing the tip to collector distance too much meant that a significant proportion of the fibres would be collected onto an unwanted surface, making the experiments much more time consuming. This meant that the maximum collector distance tested distance was 20 cm.

The tip to collector distance was varied between 8 and 20 cm for some of the initial solutions. The fibres created at shorter distances were distinctly thicker than the fibres created if the collector was further away from the needle. Once it was seen that the solutions can be spun at 20 cm, it was decided to fix that variable.

The voltage was also varied between 15 and 30 kV for most solutions in the preliminary study to determine the range of voltages where fibres could be spun. For some solutions, there was either one voltage that gave significantly better results than other voltages. For other solutions, there was a range of voltages that gave good fibres. Different voltages were tested with a step of 1 kV to 3 kV between different runs of the same sample.

The minimum voltage of 15 kV was chosen, as lower values were unable to initiate a jet. The maximum voltage tested depended on the solution, as there was an upper bound after which the jet became very unstable without a straight section near the needle. This resulted in the jet also being discontinuous as the Taylor cone receded into the needle. The feed rate was increased to counter the receding Taylor cone, but that did not always solve the problem and even if it did, the fibres had larger diameters due to the initial jet being thicker. And sometimes the solvent was unable to evaporate fully and fused fibres were created on the collector.

Different solutions required slightly different voltages for optimal spinning, however the optimal voltage range in general remained between 18 kV and 24 kV.

Feed rates of 0.05 ml/hour to 1 ml/hour were tested for different solutions and voltages. The feed rates were adjusted to keep the Taylor cone stable so that continuous fibres could be created. In general, the appropriate feed rates were between 0.15 ml/hour to 0.4 ml/hour. This variable was also not fixed for the final experiments. Due to the relative humidity and the solution viscosity changing from sample to sample, it made little sense to keep this variable fixed, because it was more important to find a setting that is capable of producing continuous fibres with a specific solution in that specific humidity.

The needle was chosen to be a 23G needle. Options of 19G to 23G were available and two of them were tested. As no difference was seen from the initial experiments, 23G was chosen due to it being the one with a larger inner diameter to avoid larger shear forces inside the needle and complicating the study even further. The process already has a big number of variables, and the safest available choice was taken to increase the likelihood of success.

Another parameter that was tested was the collector. Different setups were tested for collecting fibre mats. A glass slide with dimensions of 2 cm by 8 cm was tested, but as a non-conductive material it repelled the fibres, and it was an inefficient way to collect a significant amount of fibres as the yield was low. The second issue with this method was in separating the fibres from the slide. An aluminium foil solved the problem of low yield as it conducts the charge away and the fibres can be collected at a higher rate. However, it was very difficult to separate most fibres from the aluminum foil. These setups also weren't able to create fibres that are well aligned.

The eventual solution was to create a setup as shown in Fig. 3.1. That allowed the collection of fibres at a good rate with a relatively easy way to remove them from the collector. It did have a drawback of more material being collected where the collector was and not as much in the air gap between the collector lines. Therefore, it was not possible to get a fibre mat that has a uniform thickness.

# Chapter 5

# Results and Discussion

## 5.1 Characterization of Materials

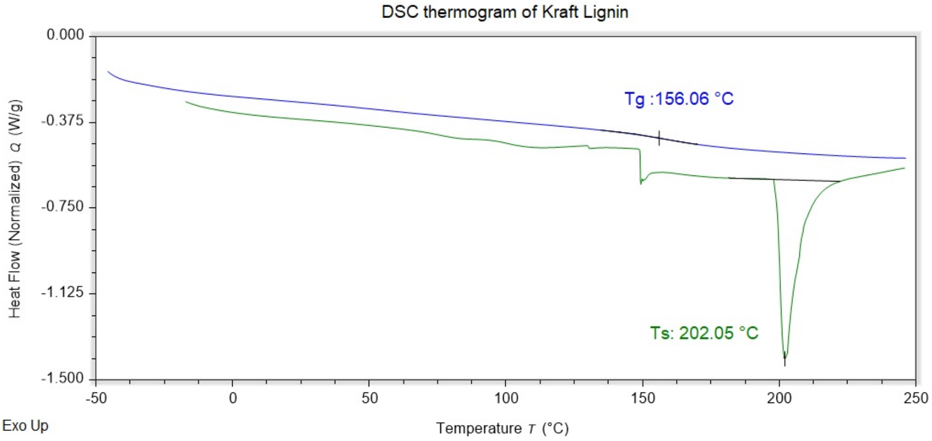

FIGURE 5.1: The DSC thermogram from the first heating (green) and second heating (blue) cycles of lignin

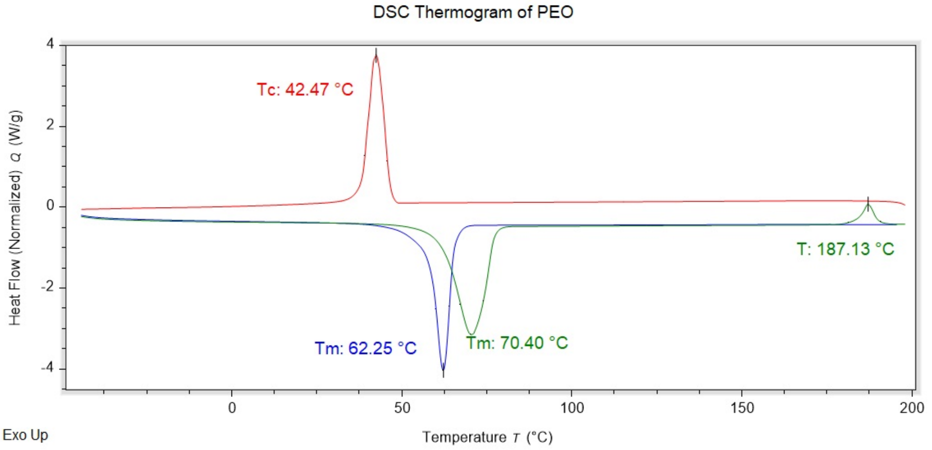

FIGURE 5.2: The DSC thermogram from the first heating (green), cooling (red) and second heating (blue) cycles of PEO

The DSC thermograms of the obtained KL is shown in Fig. 5.1. The glass transition temperature ($T_g$) marking the transition from a glassy to rubbery state was taken from the second heating cycle in order to evaporate off any water content and to remove the thermal history. This was seen at around 156°C ± 2°C and was calculated from the midpoint of the transition in the thermogram. The softening temperature ($T_s$) was shown to be at around 202°C in the first heating cycle. The softening temperature fuses the lignin molecules together and is not evident in all types of lignin as it is characteristic of a thermoplastic behaviour[143].No significant thermal events were evident in the cooling cycle. The DSC thermogram of PEO is shown in Fig. 5.2 and shows a melting temperature ($T_m$) at 70°C and 62°C in the first and second heating cycles respectively. The reduction in the value for the second heating cycle is due to the thermal history of the material being erased. The crystallisation temperature ($T_c$) was shown at around 42°C in the cooling cycle. The $T_g$ of PEO is around −70°C and is not evident in the thermogram due to the temperature limit of the equipment being above that. There is another exothermic peak at around 187°C in the first heating cycle, but it is not evident what this peak corresponds to. There could be a slight onset of decomposition at this temperature.

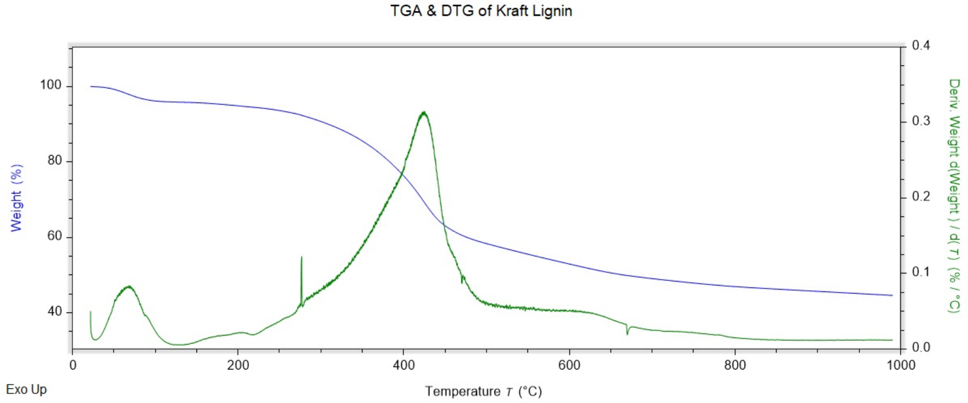

FIGURE 5.3: The TGA & DTG thermograms of Lignin

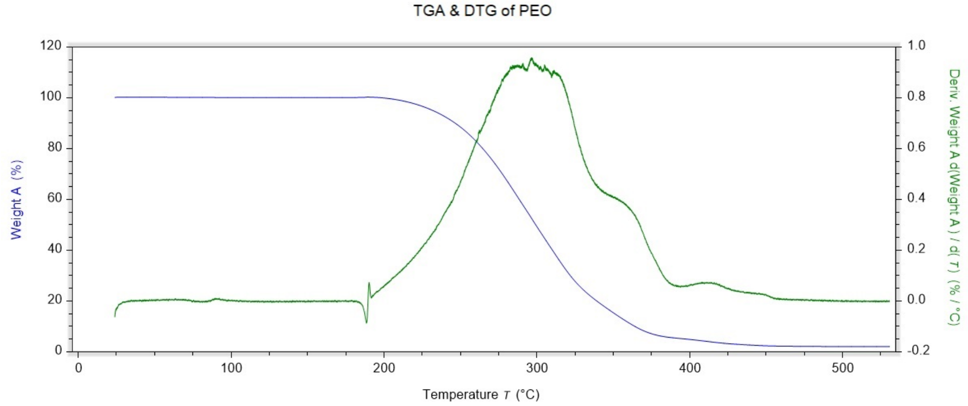

FIGURE 5.4: The TGA & DTG thermograms of PEO

The TGA and derivative (DTG) thermograms of KL and PEO are shown in Fig. 5.3 and Fig. 5.4 respectively. The DTG thermograms shows peaks where the thermal degradation happens in a rapid manner. The degradation of KL occurs in multiple stages, with the first stage occurring at 30 °C to 110 °C due to the evaporation of the absorbed water. The second stage shows a broad peak occurring from 140 °C to 320 °C and is attributed to the degradation of components of carbohydrates in the lignin and evolution of CO, $CO_2$ and $CH_4$[144]. The most rapid degradation happens from 325 °C to 425 °C due to the fragmentation of inter unit linkages and release of monomers and other derivatives of phenols into the vapour phase [145]. The broad peak occurring after 500°C is due to the decomposition of aromatic rings[146]. After heating to 1000°C, around 44wt% of the sample remains unvolatilised as highly condensed aromatic structure are formed[147]. The degradation of PEO occurs in one stage, with the maximum weight loss occurring from 215 °C to 300 °C. There was no weight loss until 200°C and had less than 5wt% of the sample remaining after 400°C.

## 5.2 Characterisation of Solution

Rotational tests were used to determine the shear viscosity as a function of shear rate for all solutions to determine the change in viscosity with different KL:PEO ratios and different total polymer content. They were also measured at two different times (2 hours and 24 hours) after combining the individual solutions of KL and PEO to study the effect of polymer chain relaxation over time. PEO with high molecular weight can relax over time, reducing its chain entanglement with KL[6].

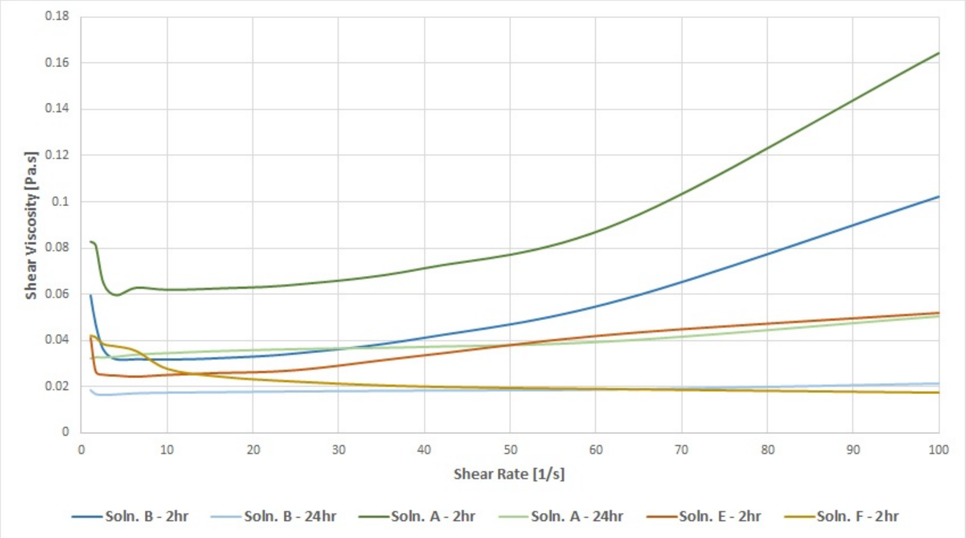

FIGURE 5.5: The shear viscosity as a function of shear rate plots of solution A, B, E and F measured 2 hours and 24 hours after preparing them

Fig. 5.5 shows the shear viscosity as a function of shear rate for solutions A, B, E and F measured 2 hours after preparing them and for solutions A and B measured 24 hours after preparing them. The shape of the viscosity curve shows a change in viscosity with increasing shear rate, indicating that they behave as non-Newtonian fluids. Solutions A, B and E exhibit shear thickening behaviour while solution F exhibited shear thinning behaviour. This could be due to solution F having the least amount of PEO and exhibiting properties similar to that of a pure KL solution. Solution A had the highest viscosity value followed by B, E and F. This is in direct relation with the higher ratio of PEO and higher overall polymer content in the solutions. The viscosity measurements after 24 hours of preparation of solution A and B shows a reduction in the viscosity values. This is due to PEO chains relaxing and getting disentangled[148, 149]. These measurements for solution E and F taken 24 hours after solution preparation is not reported as they were below the equipment limits. However, it is evident that all four solutions exhibited a reduction in shear viscosity after being stored for 24 hours.

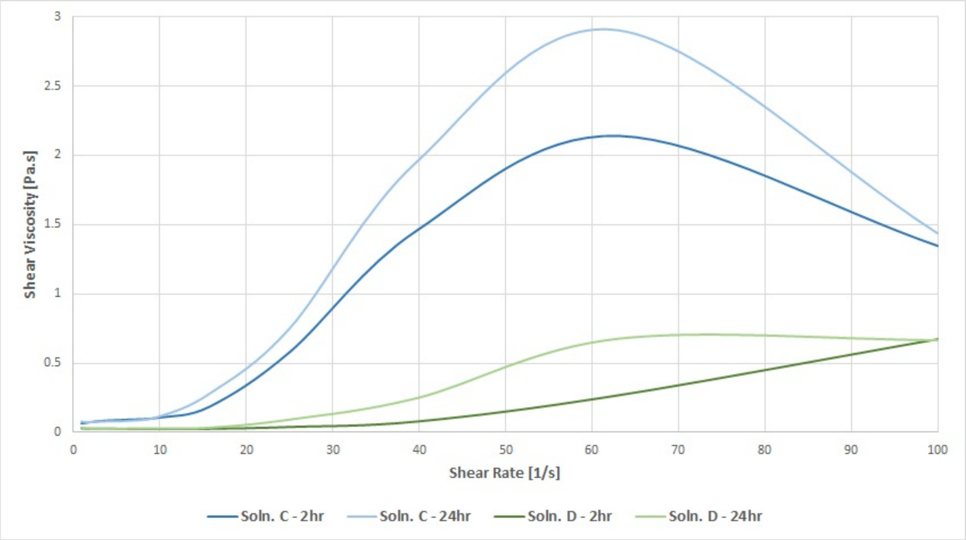

Figure 5.6: The shear viscosity as a function of shear rate plots of solution C and D measured 2 hours and 24 hours after preparing them

Fig. 5.5 shows the shear viscosity as a function of shear rate for solutions C and D, measured 2 hours and 24 hours after preparing them. The viscosity value of solution C is higher than D, with both of them having significantly higher values than the other four solutions. This again is directly related to the Lignin:PEO ratio and the overall polymer content in the solutions. Both the solutions exhibit shear thickening behaviour similar to the previous ones. However, solution C exhibits a shear thinning behaviour above shear rate of $60s^{-1}$. These measurements were taken on the log scale, with the second last measurement taken just above a shear rate of $60s^{-1}$. It was observed during the experiment that the solution would form a gel and flow out of the geometry gap. The reduction in the viscosity values could be due to this phenomenon. Similar behaviour was also observed for solution D when measured after 24 hours.Both solutions also exhibit higher shear viscosity value after being stored for 24 hours. This could be due to the fact that at such high concentrations, the solutions have a higher tendency to form a gel[6].

It can be observed that the storage time of KL&PEO solutions have a significant effect on their viscosities and thereby on their electrospinnability.

Out of the combinations of the three lignin:PEO ratios and three overall polymer contents, just five solutions were spinnable. The others were tested, but did not produce fibres. Out of the solutions with 6 % overall polymer content the lignin:PEO ratio of 93:7(sample E) resulted in fibres, the lignin:PEO ratio of 95:5 electrosprayed and the 97:3 was therefore not going to be viscous enough either. Out of the solutions with 8 % overall polymer content, the solutions with the lignin:PEO ratio of 95:5(sample B) and 93:7(sample A) created fibres, while the solution with a lignin:PEO ratio of 97:3 electrosprayed. Out of the solutions with 10 % overall polymer content, the lignin:PEO ratios of 97:3(sample D) and 95:5(sample C) created fibres, while the solution with the ratio of 93:7 was too viscous to spin.

## 5.3 Morphology of the Fibres

The morphology of the fibres was characterised with SEM analysis. For samples A and B the fibres were imaged after spinning, after stabilisation and after carbonisation. Samples C, D and E were imaged only after carbonisation. The two samples were characterised at each step to show the evolution of the fibres throughout the process and to see whether the evolution of the fibres from different solutions is similar or not. The rest of the samples were not imaged at all steps as the two samples gave a good enough overview of the process and the production of samples for imaging takes a significant amount of time.

In Figure 5.7 the distribution of the fibre diameters at the three stages of the carbon fibre production for solution A can be seen. The average fibre diameter for the electrospun fibres for sample A is 1.56 microns, which reduces to 1.28 microns for the stabilised fibres and 0.57 microns for the carbonised fibres.

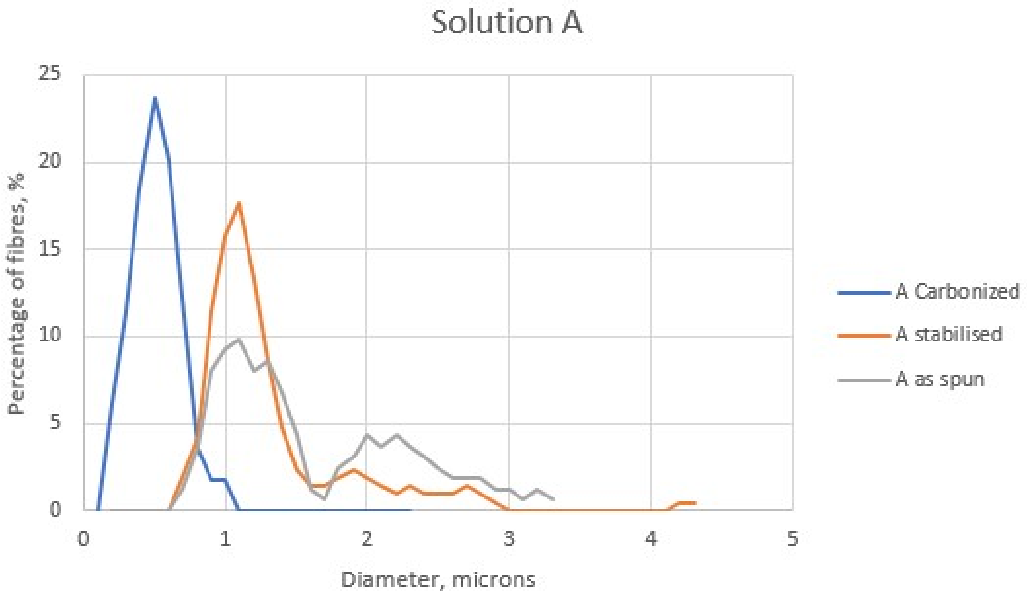

FIGURE 5.7: The distribution of fibre diameters for sample A at the different stages of the carbon fibre production process.

The figure 5.8 shows the corresponding results for sample B. The electrospun fibres have an average diameter of 0.82 microns, which reduces to 0.49 microns for the stabilised fibres and to 0.42 microns for the carbonised fibres.

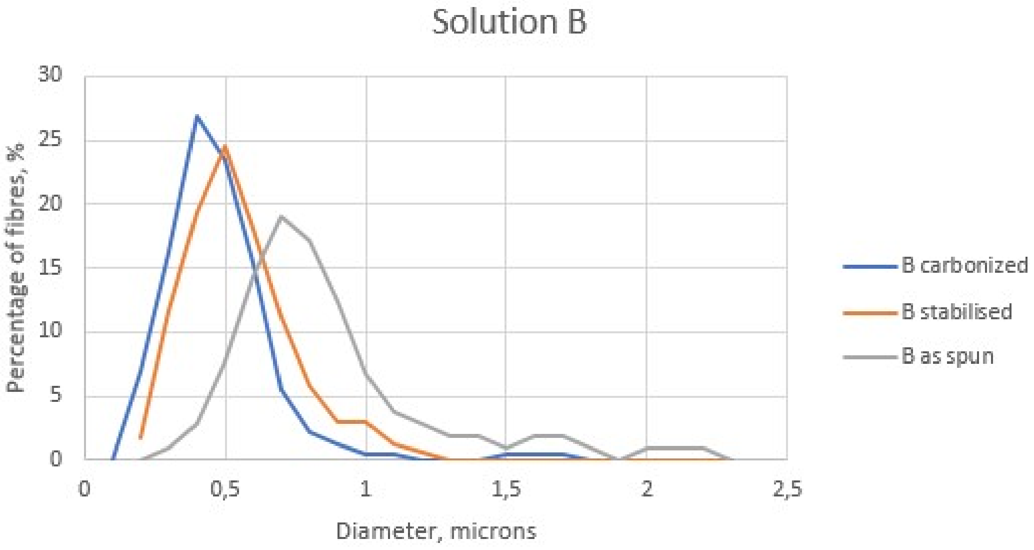

FIGURE 5.8: The distribution of fibre diameters for sample B at the different stages of the carbon fibre production process.

The diameters of the fibres decrease during stabilisation and carbonization due to the reactions and the entropy recovery. There is a significant difference in the diameter change between the two samples studied, as the diameter of sample A decreases by about 64 % and the diameter of sample B decreases by about 49 %. There can be multiple reasons that explain this difference. One of the sources of uncertainty is the fixture used for keeping the spun mat from contracting during stabilisation and carbonization. The fixture would work well for a mat with aligned fibres of uniform thickness. However, that was not possible to realise with the collector configuration used in this study. Therefore, it is not clear whether the fibre mats were held from contracting to a similar degree or whether they contracted a different amount.

Another significant detail with regard to the contraction is that while the collector was able to collect reasonably well aligned fibres for a while at the start of spinning, soon the fibres became randomly aligned as the mat grew thicker. As the fixture held the fibres from two sides, the randomly oriented fibres were not tightly held from all sides and could contract in one direction. And as the thickness of the fibre mats inevitably varied as it was not possible to control, and that is likely to introduce uncertainty to the measurements.

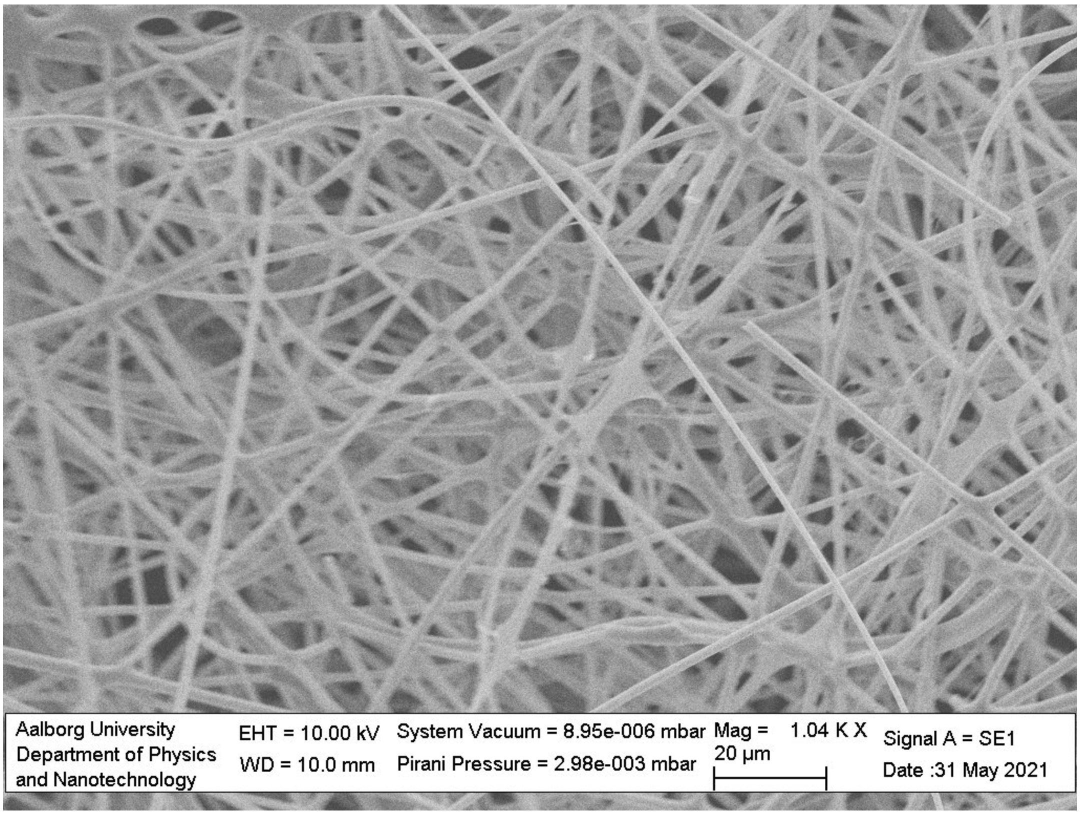

FIGURE 5.9: Sample A at a magnification of 1000x.

In Figure 5.9 a sample of solution A is shown after spinning. It is clear that the fibres in this image are not oriented and some of the fibres have fused together as can be seen on the right side of the image for example. The fibre diameters are generally within a reasonably narrow range, with the main source of the diameter difference coming from the fusion of fibres.

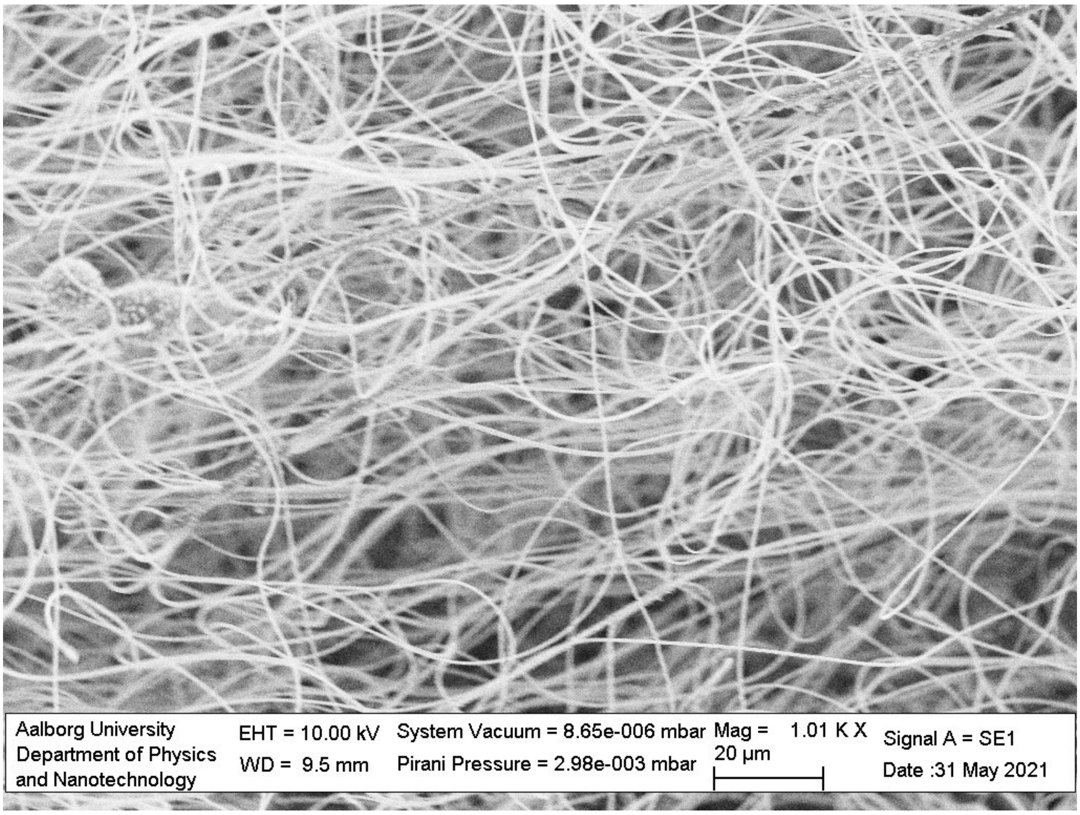

FIGURE 5.10: Sample B at a magnification of 1000x.

In Figure 5.10 a sample of solution B is shown after spinning. The fibres are generally uniform in diameter, with a few exceptions. In this image about a third from the top one thicker fibre can be seen, which also contains a bubble-type of a formation and has some sort of particles on the surface of the fibre. The large majority of the fibres are smooth, however some of them have particles on their surface.

## 5.4 Characterisation of Carbonised Fibers

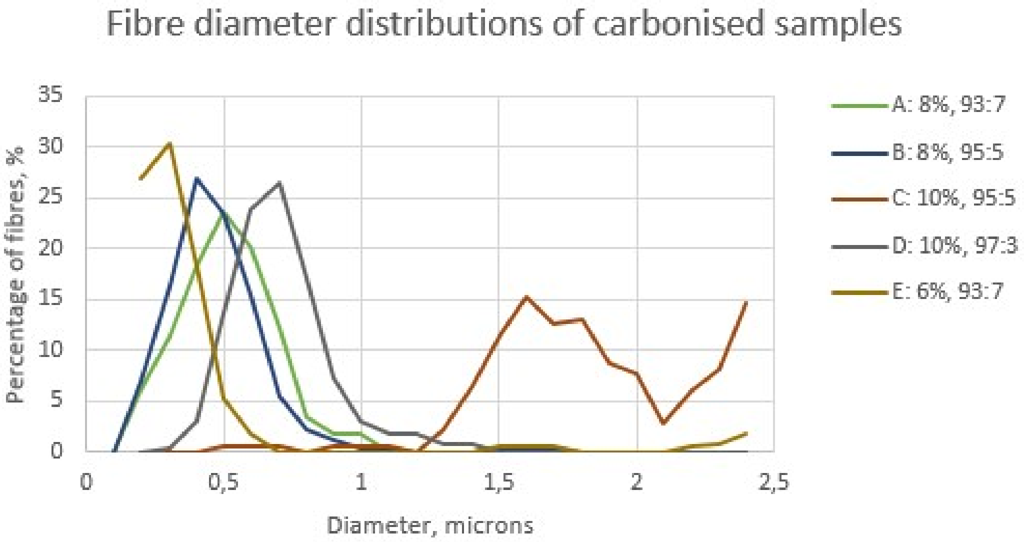

Figure 5.11: The distribution of carbonized fibres sizes for the samples A, B, C, D and E.

In Figure 5.11 the distributions of the fibre diameters are shown. Solution C has the biggest average diameter of 1.82 microns. This is expected as the viscosity of that solution is significantly higher than the other solutions and the jet is not stretched as much as the jets of the other solutions. The other fibres had diameters in the range of 0.31 microns to 0.65 microns, with solution E having the thinnest diameter. The diameters of the carbonised fibres can be seen in Table 5.1.

Table 5.1: The average fibre diameters of the studied solutions

| Solution | Average diameter, microns |
|---|---|
| A - 93:7, 8% | 0.47 |
| B - 95:5, 8% | 0.42 |
| C: 95:5, 10% | 1.82 |
| D: 97:3, 10% | 0.65 |
| E: 93:7, 6% | 0.31 |

The fibre diameters are reasonably well correlated with the measured viscosity of the solutions. The decrease in viscosity results in the decrease in the fibre diameter as well. This is an expected result as the theory also suggests that lower viscosity results in fibres with smaller diameters. However as can be seen from the images of Sample E in 5.16, there is a limit to how much the viscosity can be decreased as the fibres created with these parameters were not uniform any more.

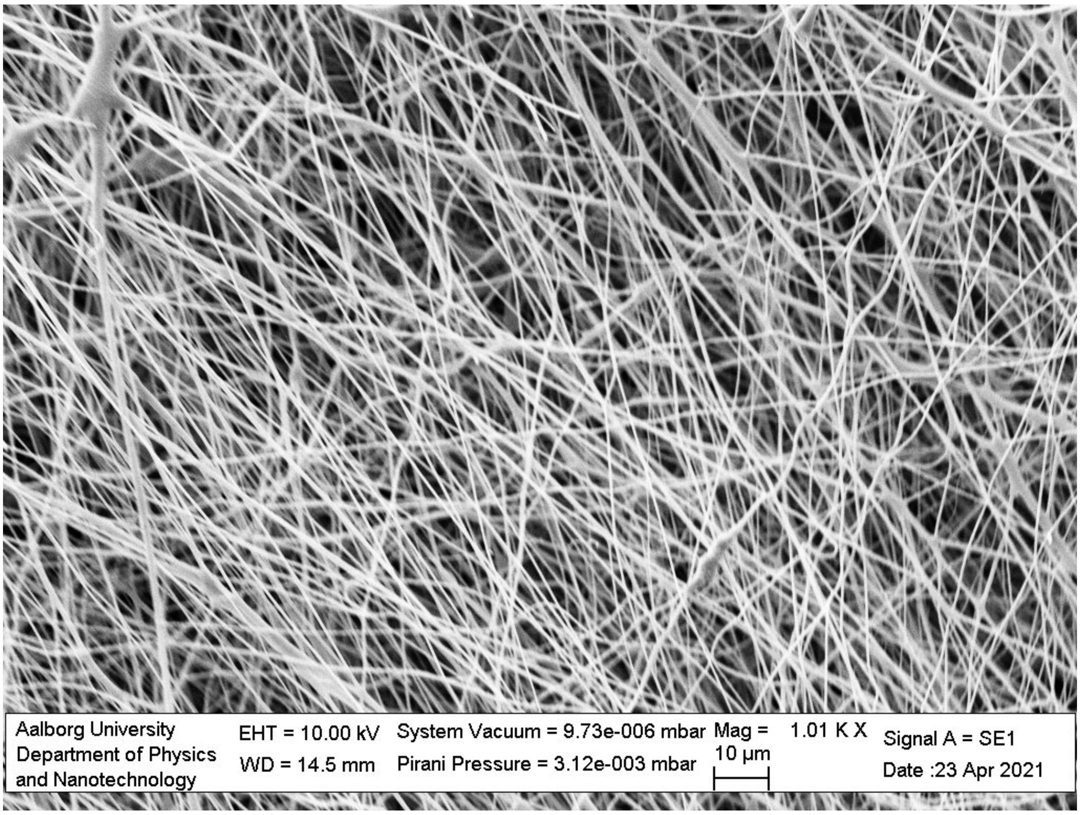

Figure 5.12: Carbonized sample A

In Figure 5.12 the carbonized fibres of solution A are shown. The fibres have a rather wide range of diameters with an average of 470 nm and a standard deviation of 160 nm.

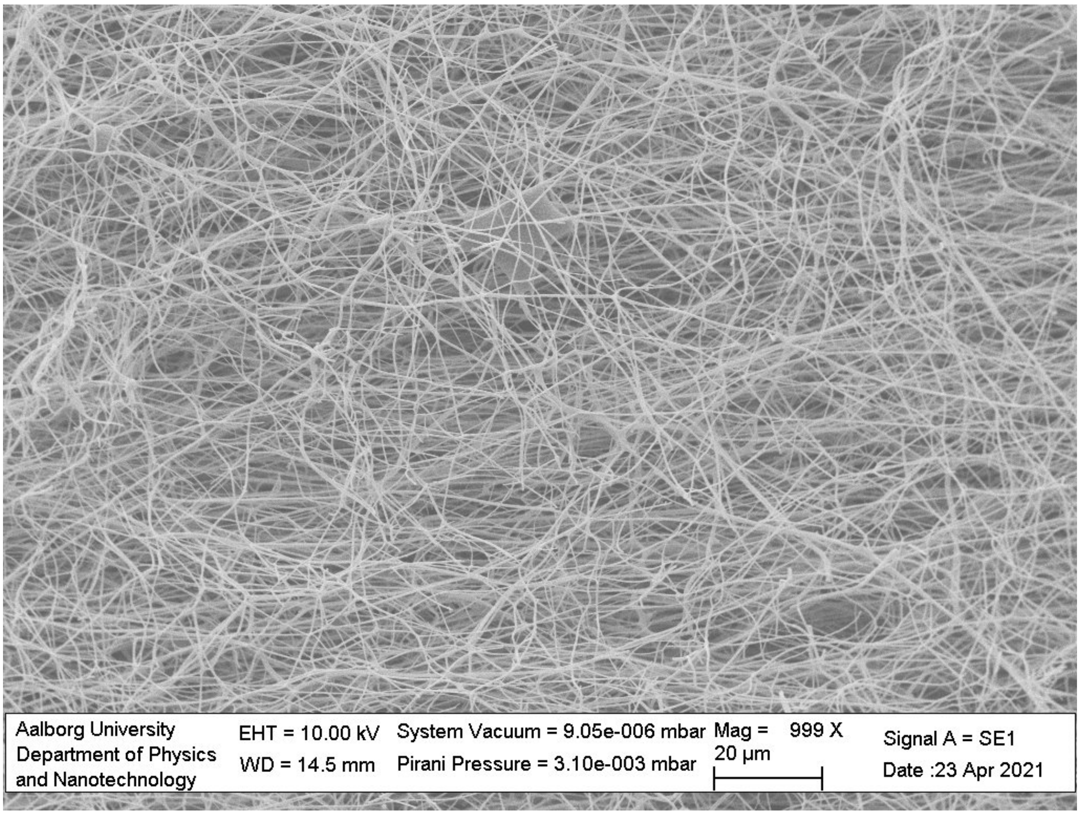

FIGURE 5.13: Carbonized sample B

In Figure 5.13 the carbonized fibres of solution B can be seen. The fibres have a reasonably narrow range of diameters, with the average diameter being 420 nm and the standard deviation being 190 nm. The fibres are reasonably uniform and while there is a small amount of fibres that have been fused together, it is generally something that happens rarely rather than often.

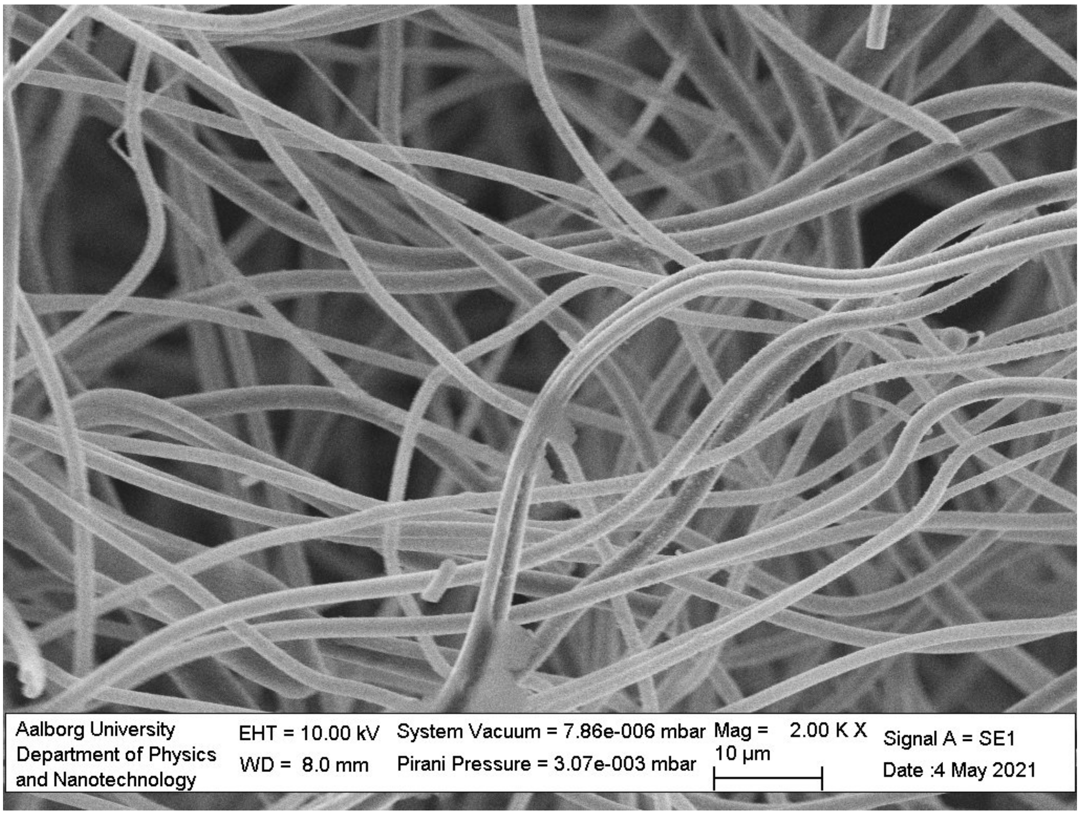

FIGURE 5.14: Carbonized sample C

In Figure 5.14 the carbonized fibres of solution C can be seen. It has to be noted that while the magnification of the other images in this section are with a similar magnification, then this figure has a higher magnification, which means that the fibres have a much larger diameter of 1.82 microns with a standard deviation of 620 nm. The fibres are quite uniform and the fibres do not experience significant fusion.

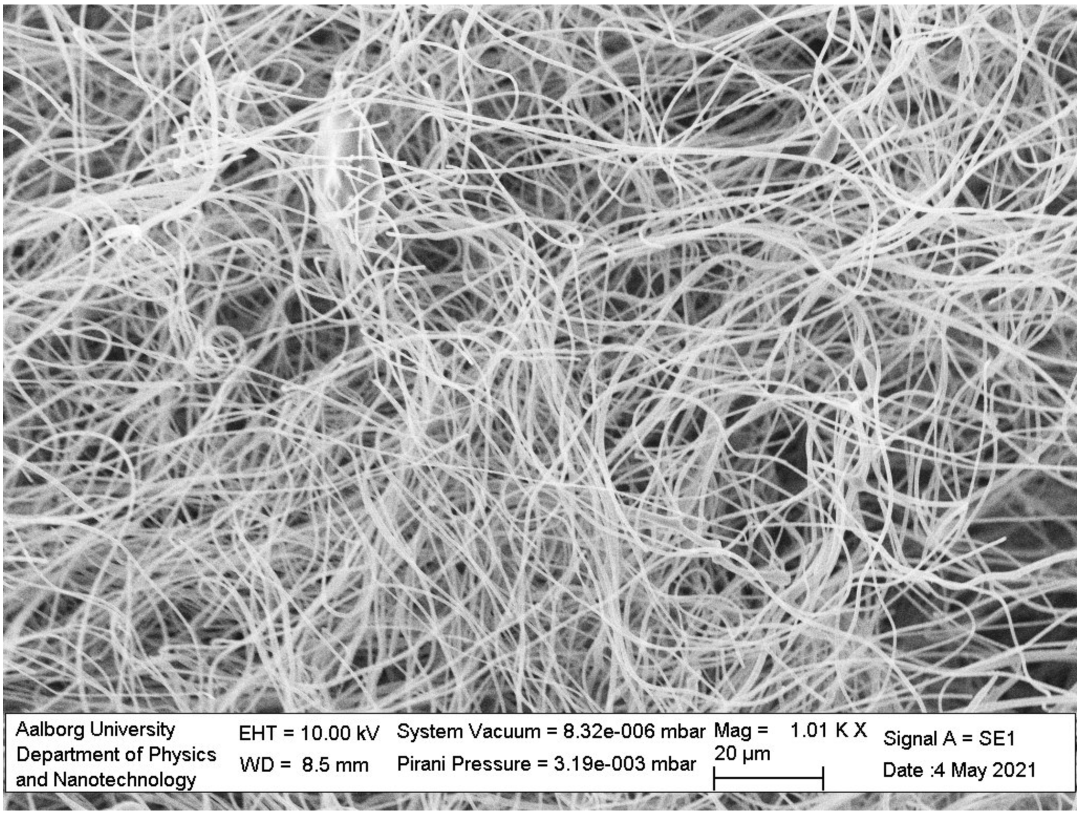

FIGURE 5.15: Carbonized sample D

In Figure 5.15 the carbonized fibres of sample D are shown. The fibres have a diameter of 650 nm with a standard deviation of 160 nm. The fibres are therefore quite uniform in their diameter and have smooth surfaces.

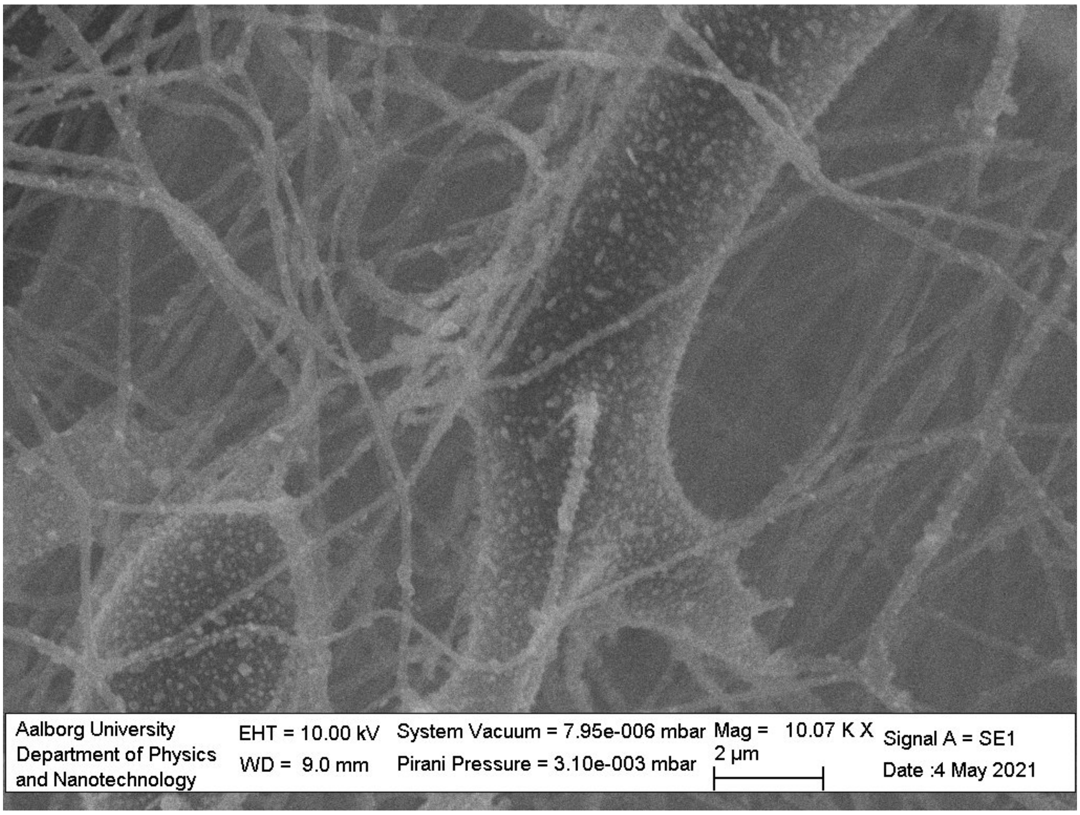

FIGURE 5.16: Carbonized sample E

In Figure 5.16 the carbonized fibres of sample E are shown. This image is done with a higher magnification, because the lower magnifications were unable to show the details of the fibres well enough. These fibres have the lowest average diameter of 310 nm, however their standard deviation is huge with 490 nm and the image shows why this is. The standard deviation does not make too much sense in a way, because the fibre mat consists of fibres with diameters in the 150 nm to 300 nm range and then fewer very large fibres with diameters of around 3 microns. The image also shows that the fibres are not smooth on their surface as there are some smaller particles on the surface of most, if not all fibres.

### Raman spectroscopy

The Raman spectra helps us study the structure of carbon present in the carbonised fibres of all five samples. All samples were carbonised at the same heating rate, temperature and duration.

The Raman spectra is deconvoluted to four peaks: two Lorentzian peaks in the range of 1290 to 1350 cm$^{-1}$ and 1580 to 1600 cm$^{-1}$ for the D and G bands respectively, and two Gaussian peaks in the range of 1110 to 1120 cm$^{-1}$ and 1500 to 1550 cm$^{-1}$ for the D4 and D3 bands respectively. The D band indicates the presence of polycrystalline graphite and represents a turbostratic carbon structure where the carbon atoms are disordered around the graphite sheets. The G band represents the carbon structure in a single crystal of graphite and is due to the in-plane vibrations of carbon atoms. This band is more prominent in highly graphitised materials. The D4 and D3 band have been assigned to the presence of impurities in the graphitic structural units and amorphous carbon respectively.

The intensities ($\mathrm{I}_D$, $\mathrm{I}_G$) and normalised areas ($\mathrm{A}_D$, $\mathrm{A}_G$) of the D and G bands are used to characterise the graphitic structure in all samples. The full width at half maximum (FWHM) of these bands also provide valuble information as FWHM decreases with increased ordering in the structure. These values for all five samples are mentioned in Table 5.2 and was taken as an average of five measurements.

Table 5.2: The centre position, FWHM, intensity and normalised area of D and G bands for all five samples

| | D Band | | | | G Band | | | |
|---|---|---|---|---|---|---|---|---|
| Sample | Center [cm$^{-1}$] | FWHM | Intensity ($\mathrm{I}_D$) | Area ($\mathrm{A}_D$) | Center [cm$^{-1}$] | FWHM | Intensity ($\mathrm{I}_G$) | Area ($\mathrm{A}_G$) |
| A | 1344.76 | 229.65 | 5058.4 | 1823793.3 | 1588.2 | 95.81 | 4069.45 | 613741.3 |
| B | 1344.14 | 215.6 | 3570.96 | 1198144 | 1591.46 | 92.8 | 2652.02 | 396087 |
| C | 1345.4 | 221.2 | 3447 | 1203014.6 | 1588 | 101.6 | 2987.6 | 476012.2 |
| D | 1344.38 | 211.2 | 4247.6 | 1362890.2 | 1586.56 | 105.2 | 3765 | 604979.8 |
| E | 1348.7 | 244 | 3750.4 | 1405186.8 | 1589.48 | 104.88 | 3243 | 572357.6 |

The data in the above table shows that the centre positions of the D and G bands were very similar for all the samples, as these values mostly change with the carbonisation temperature or heating rates. The FWHM values of the D bands showed higher values for samples with higher amounts of PEO with the same overall polymer content. This trend was also seen in the FWHM of the G bands, with sample D being an exception. This could suggest that the samples with lower amounts of PEO had more ordered structure. The R value is a better parameter for comparing the samples and is discussed below.

The ratio of the intensities or areas of the D and G bands provide us with the R value, which indicates the degree of graphitisation and ordered structure. Multiple studies have reported the R value based on the intensity of the D and G bands. However, several authors also use the term "relative intensity" when referring to the normalised area. In this report, we have reported the R values based on both of them. The R value is also used to calculate the graphitic mole fraction ($x_G$) and the crystallite size ($L_a$) and are shown in Table 5.3.

Table 5.3: The R value, graphitic mole fraction and crystallite size calculated from the intensity and area for all five samples

| | From Intensity | | | From Area | | |
|---|---|---|---|---|---|---|
| Sample | R ($I_D/I_G$) | $x_G$ | $L_a$ [nm] | R ($A_D/A_G$) | $x_G$ | $L_a$ [nm] |
| A | 1.250 | 0.445 | 15.444 | 3.004 | 0.251 | 6.457 |
| B | 1.377 | 0.421 | 14.083 | 3.255 | 0.240 | 6.152 |
| C | 1.154 | 0.464 | 16.667 | 2.514 | 0.285 | 7.658 |
| D | 1.165 | 0.463 | 16.605 | 2.338 | 0.301 | 8.307 |
| E | 1.154 | 0.464 | 16.663 | 2.722 | 0.27130 | 7.193 |

The R value calculated based on the intensity and areas show a significant difference in the values. The values obtained from the areas are almost twice that of obtained from the intensity. When comparing the R values for sample A and B, sample A shows a higher degree of graphitisation from both the intensity and area based calculations.

This would suggest that higher amounts of PEO increased the degree of graphitisation. Sample A also had a higher value of $x_G$ and $L_a$ compared to B. When comparing the values for solution C and D, the R values are slightly lower for sample C when using the intensity values and lower for sample D when using the area values. However, when compared to the previous samples (A and B) they have a lower R value suggesting that with higher contents of lignin, the carbon structure is more ordered. The $x_G$ and $L_a$ values for C and D are quite similar when calculated from intensity. But, when calculated from area, sample D has a higher value. Sample E also had a very low R value, even though it had a much lower amount of lignin. The results from the Raman data do not follow any natural trend to be correlated with the varying amounts of PEO and lignin.

Overall, the carbonised samples C and D gave a lower R value irrespective of the method used. The R values of reported across the literature for lignin based CF are within the range that was found in this study. This is also because the authors were not clear about which method was used.

### X-ray diffraction

The XRD diffractogram was performed on the powdered samples for samples A, B, C and D. However, this did not result in a peaks in the diffractogram that corresponds to the literature. Goudarzi et al. conducted XRD analysis on KL derived CF and reported that a measurement time of 12 hours was required to increase the resolution and obtain peaks in the diffractogram[150]. A measurement time of 6 hours was chosen to check if it would result in a better diffractogram. However, the XRD equipment had several issues with such long measurements and would fail to complete the measurement. Hence, XRD diffractogram was obtained for just one sample (sample A). The equipment was later under repair and further measurements could not be done.

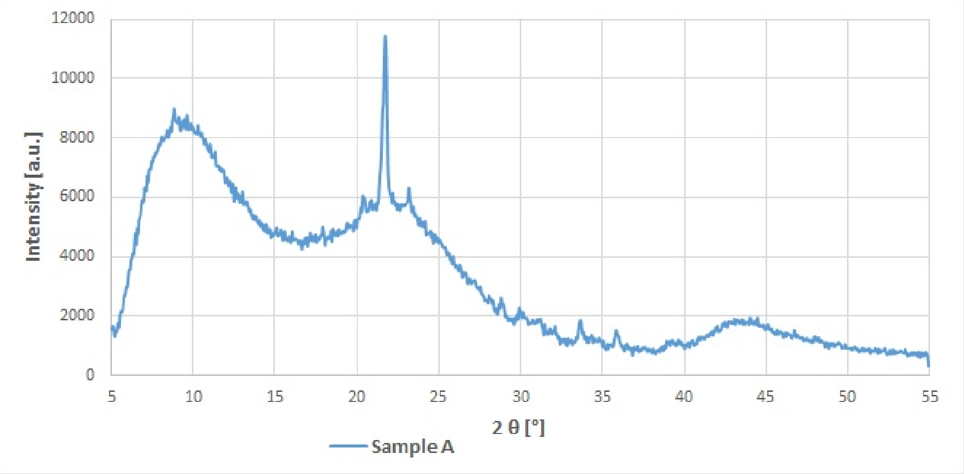

FIGURE 5.17: The XRD of sample A carbonised

The XRD diffractogram of carbonised sample A is shown in Fig. 5.17. A broad peak spanning from 15° to 30° with a narrow peak at $2\theta \approx 22$ was obtained. This corresponds to the (002) crystallographic plane of graphite[151]. Another small peak is visible from 42° to 47° with the maximum at $2\theta \approx 44$ and is related to the diffraction from (100) planes[152].

The interlayer spacing $d_{002}$ indicates the degree of packing in the crystal structure and was found to be 0.2056 nm for the above mentioned sample. Poursorkhabi et al. carbonised electrospun fiber mats of organosolv lignin and PEO in the ratio 95 : 5 at various carbonisation conditions and reported values between 0.379 and 0.390 nm[153]. The value obtained is lower than values that could be found in the literature. The crystallite size $L_a$ was found to be 0.02 nm and is not a reliable value. The reason for such low values could be due to the peak visible from 5° to 15° hampering the baseline correction procedure. No literature could be found for lignin based carbon fibres where this peak was visible. Further analysis has to be done in order to properly report the results from XRD.

## 5.5 Characterisation of Activated CFs

The activated CFs were characterised in two ways. The morphology of the fibres was studied by imaging them with a SEM and their ability to absorb $CO_2$ was analysed by an adsorption test.

The carbon fibres were activated at 800 °C for three different time periods: 1 hour, 30 minutes and 15 minutes. Literature[97–99, 154] suggested activation with $CO_2$ for longer periods and higher temperatures would produce fibres with bigger specific areas, however the first try with 4 hours at 1000 °C made the whole fibre mat react with the gas and disappear. This was due to the highly amorphous nature of the fibres produced in this study. Therefore shorter activation times were tested. As can be seen in Figure 5.18, the fibres had fused together even after one hour and the result could not be classified as a fibre mat any more. The sample activated for 1 hour also had very low yield with about 90 % to 95 % of the matter lost during the process.

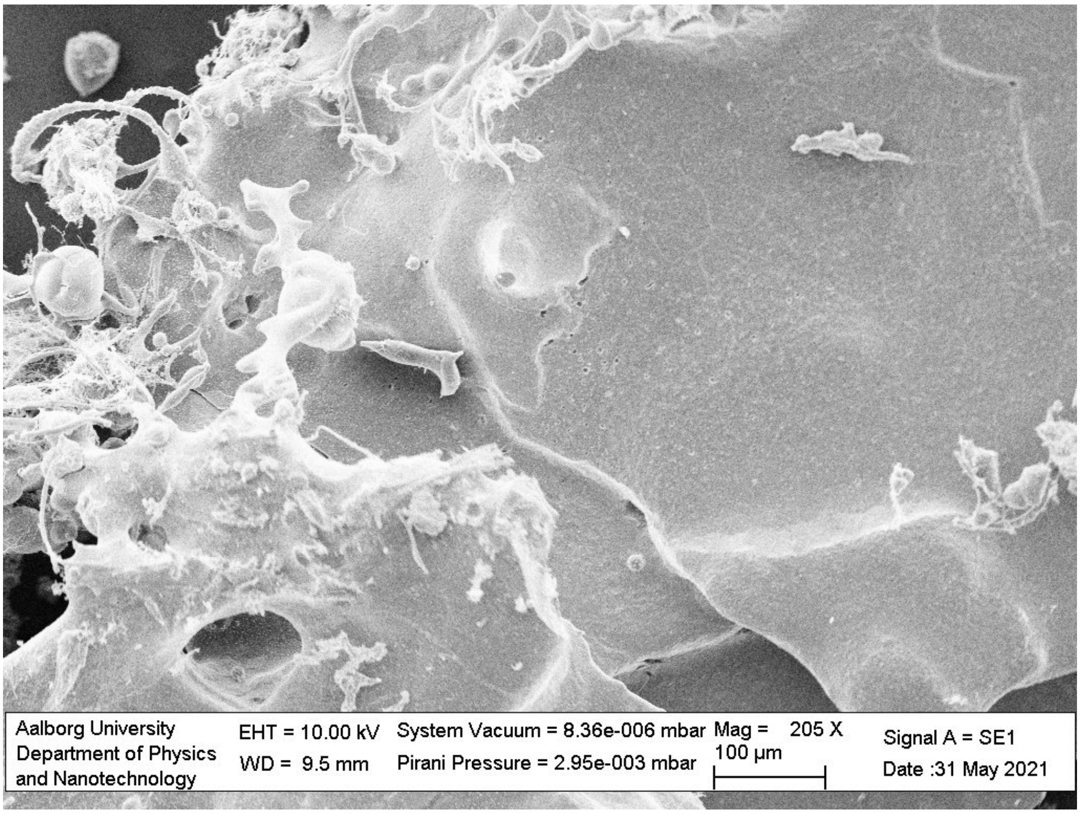

FIGURE 5.18: Sample B activated in $CO_2$ for 1 hour.

At an activation time of 30 minutes the fibres were not melted together any more as can be seen in Figure 5.19. However they had some fibres that looked like they had fused together. The yield of the activated fibre was also still very low and did not give a fibre mat of desired size, so an even shorter activation time was tested to get a high enough yield with our means to be able to test the $CO_2$ adsorption of the samples. In 5.19 it must be mentioned that there are some impurities on the sample image that make it look worse than it is due to a problem with gold coating the samples as the coating did not turn out uniform and a lot of surface artifacts were created. As the process to create a sample takes a long time and the yield was low, then it was not redone.

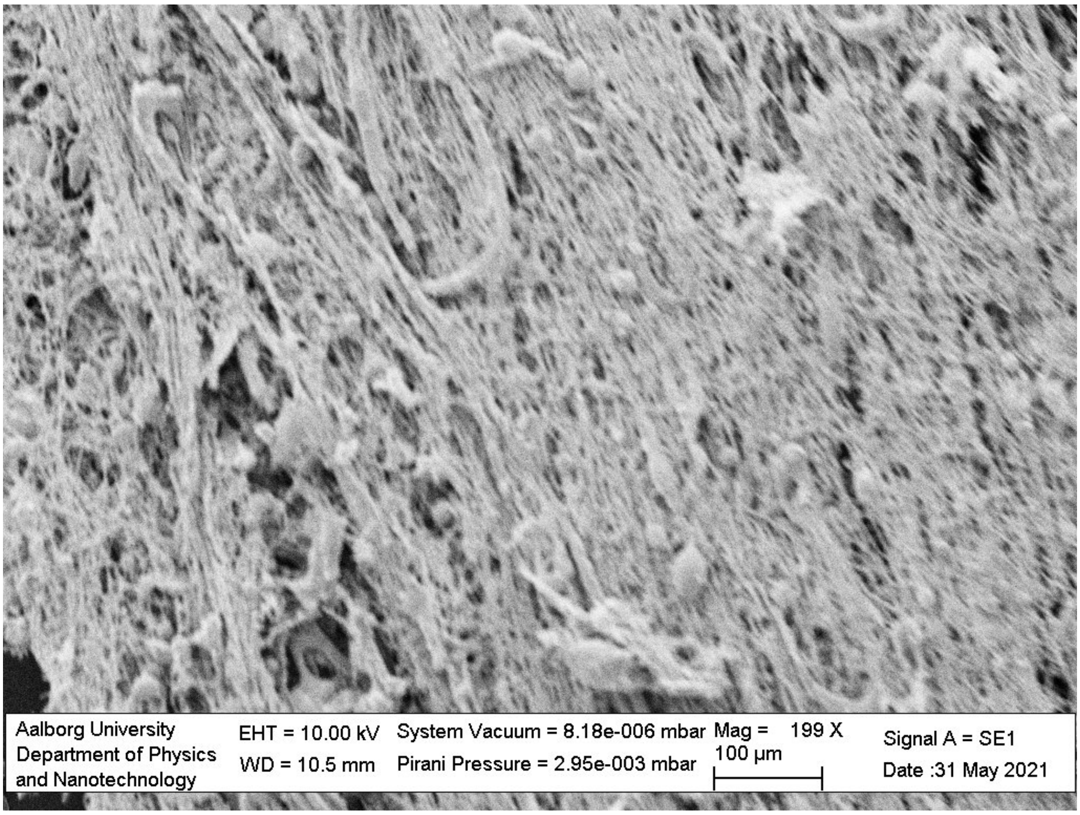

FIGURE 5.19: Overview image of sample B activated in $CO_2$ for 30 minutes.

Sample B activated for 15 minutes had a mixture of thin fibres, fused fibres and some sprayed matter as can be seen in Fig. 5.20. The difference between the same sample carbonised and activated is likely to be due to changes in the process. There was a difference in humidity when the two samples were created, with the humidity being 43.1 %, when the activated fibres were spun and 28.4 %, when the carbonised fibres were spun. Therefore, it is not clear whether the activation process had a significant effect on the fibres or whether the humidity had an effect or whether it was the combination of the two.

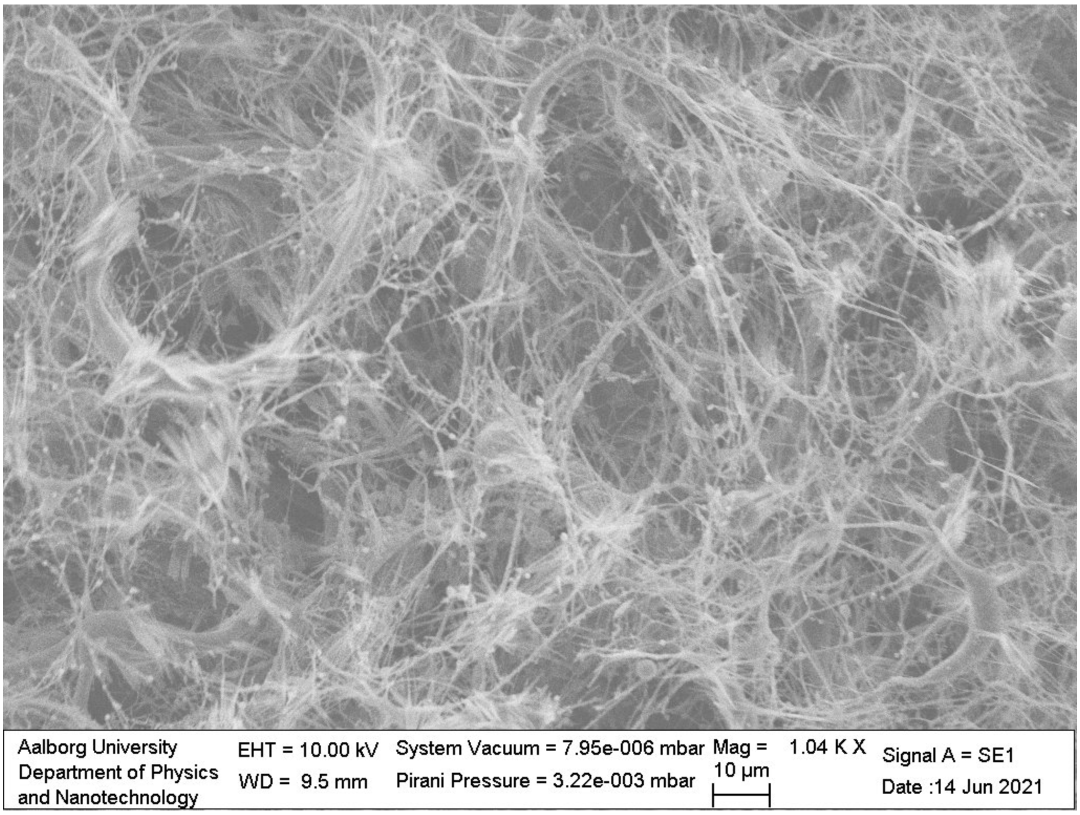

FIGURE 5.20: Sample B activated for 15 minutes in $CO_2$.

In Figure Fig. 5.21 an image of sample A can be seen. The fibres are not continuous, however the fibre mat is still intact as one piece. A small amount of fibres in this sample have fused together, which could be the result of differences in the spinning parameters. There are small differences in the spinning parameters due to the humidity of the spinning setup not being controllable. The fibres characterised in Section 5.3 about carbonised fibres were spun at a relative humidity of 26.8 %, while the activated fibres were spun at a relative humidity of 39.7 %. For the carbonised fibres a feed rate of 0.5 ml/h and a voltage of 21 kV was used, but when the same settings were tried with a higher humidity, the result was a mix of fibres and a lot of spray. Therefore, the spinning parameters were changed to allow for a creation of the best possible fibres in this environment, which turned out to be a feed rate of 0.15 ml/h and a voltage of 21 kV. It was noted even then that there was some spray present during a short trial run to determine whether the previous settings would be usable, but these settings showed most promise. This spray is visible in the image in a few places and was a likely cause for some fibres fusing together.

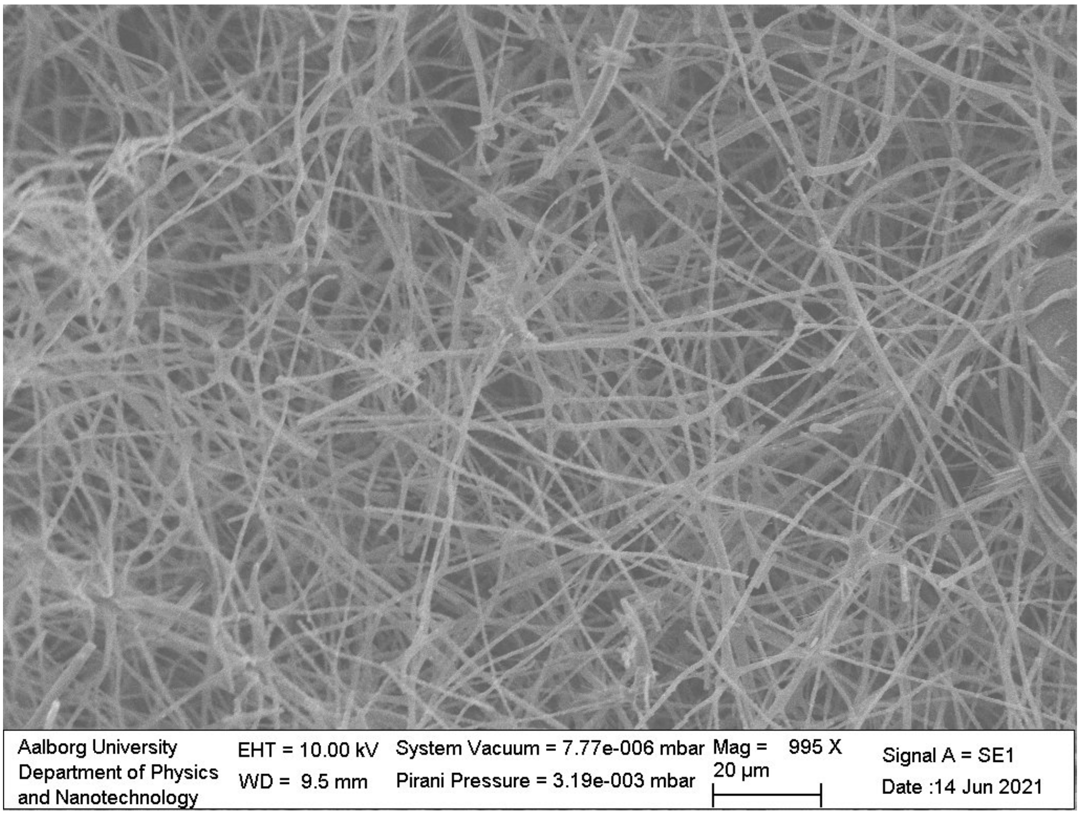

FIGURE 5.21: An image of sample A activated for 15 minutes in $CO_2$.

In Fig. 5.22 a high magnification image of sample A activated for 15 minutes can be seen. The surface of the fibres in this sample has some particles present throughout the sample. It can also be seen on the top left that some of the fibres have fused together.

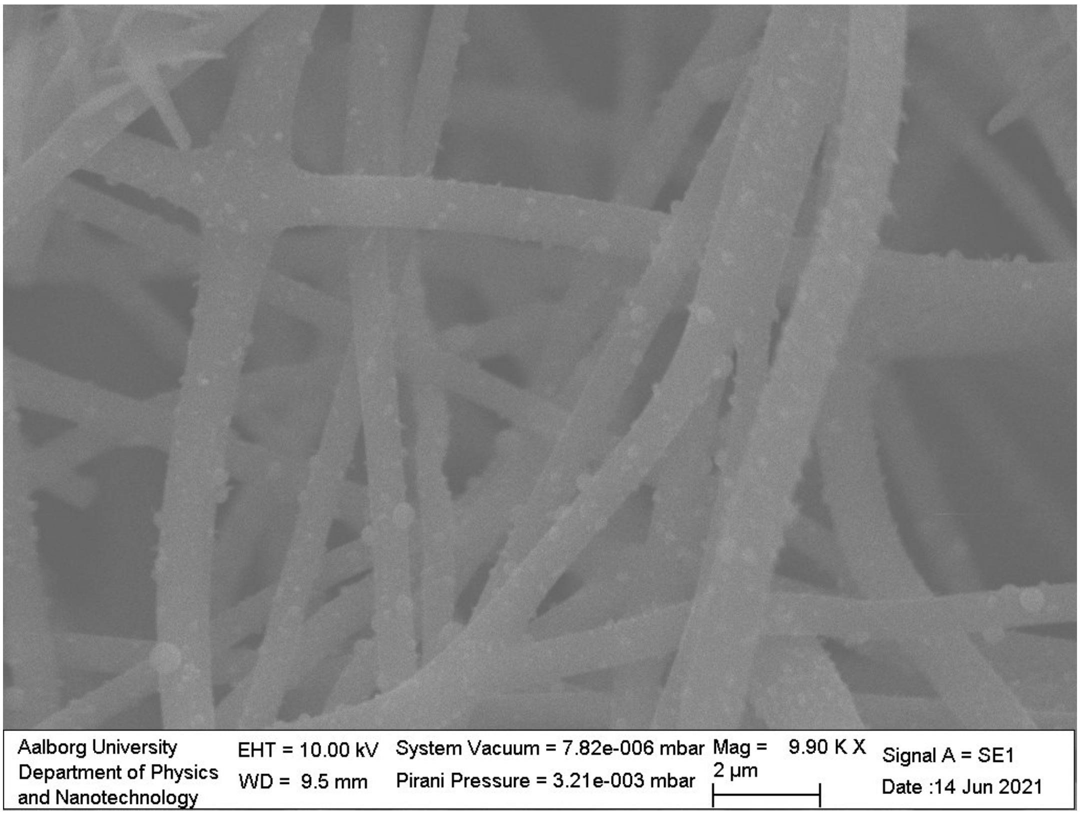

FIGURE 5.22: Higher resolution image of sample A activated for 15 minutes in $CO_2$.

The SEM analysis of the activated fibres shows that the fibres in general have retained their size and shape, however the activated fibres were more fused together and less uniform in size. This is likely because of different spinning parameters, but it's not certain that activation did not play a role. With the setup used in this project, it would have been very difficult to do a large enough quantity of fibres with the exact same parameters for all the analyses. Therefore, a certain level of uncertainty must be accounted for.

### $CO_2$ adsorption analysis

The $CO_2$ adsorption capability of the activated fibres was investigated to find out the suitability of the fibres for the application of $CO_2$ capture.

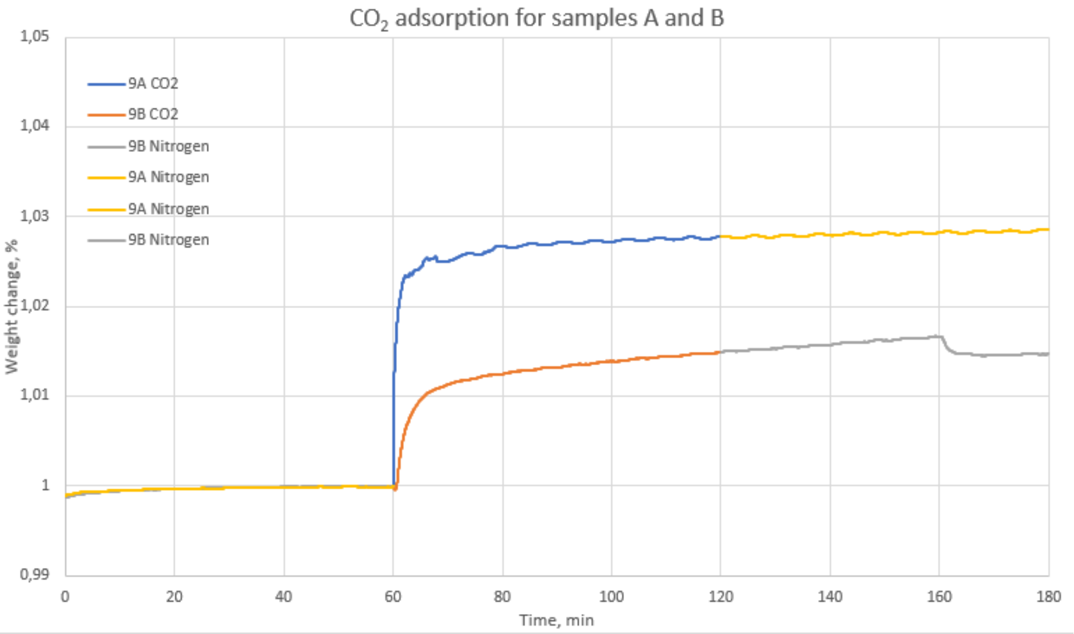

FIGURE 5.23: The adsoprtion of $N_2$ and $CO_2$ on samples A and B.

In Fig. 5.23 the fibres ability to adsorb $CO_2$ is shown. The first hour of the experiments the chamber was filled with $N_2$ and as can be seen from the graph, the mass of the sample remains unchanged. After 1 hour the gas flow was changed to $CO_2$ and the mass of the samples increases considerably, indicating adsorption of $CO_2$. Sample A sees an increase of 1.5 % in mass and sample B sees an increase of 2.8 % in mass. After 2 hours the gas was turned back to $N_2$, however no desorption of $CO_2$ was seen. This was unexpected as Li et al.[155] used a comparable method to measure $CO_2$ adsorption, and they saw a rapid desorption after changing the gas to $N_2$. The experiment suggests that the material adsorbs $CO_2$, however it remains unclear what conditions are needed to desorb it. Li et al. used a flow rate of 50L/min during the adsorption desorption analysis, with the adsorption of $CO_2$ done under a 10% stream of $CO_2$ balanced with $N_2$. Due to the limits of the equipment used in this study, a flow rate of both gases was 50ml/min. A cyclic adsorption-desorption experiment was carried out, however no desorption was recorded. The details of that experiment can be seen in Appendix B

## Chapter 6

# Conclusion

In this project activated carbon fibres were created from sustainable materials, with Kraft lignin as the main precursor material, water as the solvent and PEO as the minor constituent and the binder polymer. The effect of the solution concentrations on the fibre morphology was the main focus of the investigation. For that purpose the shear viscosity of the spinning solutions was measured, the fibre morphology of the fibres after all stages of processing was investigated. The structure of the carbon in the carbonised fibres was investigated with Raman and XRD. And the $CO_2$ adsorption capacity of the fibres was investigated in a thermal analyser.

The solution concentrations influenced the fibre morphology via solution viscosity. The solutions with higher lignin and PEO contents had higher viscosity and also created thicker fibres. At lower contents there was a minimal amount of PEO, between 2 % to 3 % that needed to be present to make the solutions spinnable, regardless of the lignin content.

The fibre diameters of the carbonised fibres were measured to be between 1.8 microns and 310 nm for the five different solutions. The thinnest created fibres had a small average diameter, but these were not uniform fibres, as the thin fibres were mixed with some electrosprayed solution and fused fibres. The other fibres were significantly more uniform, however they did also contain small amounts of spray. This is likely due to the setup not allowing humidity control and the resulting differences in the spinning parameters.

The carbonised fibres were amorphous in their structure, supported by both Raman and XRD data. This was an expected result for a carbonisation at such temperatures. The R value of the favours were almost similar for all samples, with samples that had the highest lignin content reporting the lowest R values.

The proposed application for these fibres was to be used a $CO_2$ capturing material and their suitability for this was tested in a thermal analyser. Out of the two tested activated fibres, one was able to capture 28 mg/g of $CO_2$ and another was able to capture 15 mg/g of $CO_2$. While these results do not compete with the state of the art materials for $CO_2$ capture, they still show that the activated fibres created from Kraft lignin are able to capture $CO_2$ and therefore it is a promising material for future research.

# Chapter 7

# Outlook

The main goal of this project was to successfully produce carbon fibres from lignin and PEO solutions without the use of any toxic solvents.However, the processes were far from optimised. There are multiple avenues where to direct the research on this topic.

The lignin used in this project was a commercial Kraft lignin, which has a wide molecular weight distribution. To further reduce the amount of binder polymer, fractioning the lignin could be an effective way to try and produce fibres with a better environmental impact. The carbon structure produced from fractionated lignin has been reported to be more ordered than the commercially available lignin.

The solution conductivity was a parameter that was not investigated, and increasing it could lead to fibres with smaller diameters.

The solvent used in the study was water, however it could be combined with ethanol, another relatively environmentally friendly solvent, to create fibres with different morphologies, i.e. porous or grooved fibres. This could also be combined with a coaxial needle setup, which might allow the hollow and porous fibres, increasing the specific surface area even further.

The fixture used for keeping the fibres under slight tension was tough to handle, and finding a solution that allows keeping the fibres in tension from all sides and is relatively easy to place the sample in could help improve the fibres.

Further analysis using XRD would have been beneficial as the reported data was inconclusive due to unavailability of equipment and would have helped in correlating with the Raman data.

The activation procedure was performed with $CO_2$, but the results were somewhat inconclusive and the optimal parameters for the procedure should be further studied for this polymer system.

Specific surface area measurements would be beneficial in receiving feedback about the quality of the fibres and further characterise the morphology of the activated fibres.

# Bibliography

[1] M. Norgren and H. Edlund, “Lignin: recent advances and emerging applications”, Current Opinion in Colloid & Interface Science **19**, 409–416 (2014).

[2] W. Boerjan, J. Ralph, and M. Baucher, “Lignin biosynthesis”, Annual review of plant biology **54**, 519–546 (2003).

[3] S. Laurichesse and L. Avérous, “Chemical modification of lignins: towards biobased polymers”, Progress in polymer science **39**, 1266–1290 (2014).

[4] L. Dessbesell, M. Paleologou, M. Leitch, R. Pulkki, and C. C. Xu, “Global lignin supply overview and kraft lignin potential as an alternative for petroleum-based polymers”, Renewable and Sustainable Energy Reviews **123**, 109768 (2020).

[5] D. Bajwa, G Pourhashem, A. Ullah, and S. Bajwa, “A concise review of current lignin production, applications, products and their environmental impact”, Industrial Crops and Products **139**, 111526 (2019).

[6] V. Poursorkhabi, A. K. Mohanty, and M. Misra, “Electrospinning of aqueous lignin/poly (ethylene oxide) complexes”, Journal of Applied Polymer Science **132** (2015).

[7] S. Aslanzadeh, Z. Zhu, Q. Luo, B. Ahvazi, Y. Boluk, and C. Ayranci, “Electrospinning of colloidal lignin in poly (ethylene oxide) n, n-dimethylformamide solutions”, Macromolecular Materials and Engineering **301**, 401–413 (2016).

[8] T. Ghosh, J. Chen, A. Kumar, T. Tang, and C. Ayranci, “Bio-cleaning improves the mechanical properties of lignin-based carbon fibers”, RSC Advances **10**, 22983–22995 (2020).

[9] S. Aslanzadeh, B. Ahvazi, Y. Boluk, and C. Ayranci, “Morphologies of electrospun fibers of lignin in poly (ethylene oxide)/n, n-dimethylformamide”, Journal of Applied Polymer Science **133** (2016).

[10] I. Dallmeyer, F. Ko, and J. F. Kadla, “Correlation of elongational fluid properties to fiber diameter in electrospinning of softwood kraft lignin solutions”, Industrial & Engineering Chemistry Research **53**, 2697–2705 (2014).

[11] S. Aslanzadeh, B. Ahvazi, Y. Boluk, and C. Ayranci, “Carbon fiber production from electrospun sulfur free softwood lignin precursors”, Journal of Engineered Fibers and Fabrics **12**, 155892501701200405 (2017).

[12] M. Inagaki, Y. Yang, and F. Kang, “Carbon nanofibers prepared via electrospinning”, Advanced materials **24**, 2547–2566 (2012).

[13] B. Yousaf, G. Liu, R. Wang, Q. Abbas, M. Imtiaz, and R. Liu, “Investigating the biochar effects on c-mineralization and sequestration of carbon in soil compared with conventional amendments using the stable isotope ($\delta$13c) approach”, Gcb Bioenergy **9**, 1085–1099 (2017).

[14] P. Figueiredo, K. Lintinen, J. T. Hirvonen, M. A. Kostiainen, and H. A. Santos, "Properties and chemical modifications of lignin: towards lignin-based nanomaterials for biomedical applications", Progress in Materials Science **93**, 233–269 (2018).

[15] E. I. Akpan, "Chemistry and structure of lignin", in *Sustainable lignin for carbon fibers: principles, techniques, and applications*, edited by E. I. Akpan and S. O. Adeosun (Springer International Publishing, Cham, 2019), pp. 1–50.

[16] K. Sarkanen, "Classification and distribution", Lignins-occurrence, formation, structure and reactions, 43–94 (1971).

[17] Z. Zhang, M. D. Harrison, D. W. Rackemann, W. O. S. Doherty, and I. M. O'Hara, "Organosolv pretreatment of plant biomass for enhanced enzymatic saccharification", Green Chem. **18**, 360–381 (2016).

[18] F. G. Calvo-Flores and J. A. Dobado, "Lignin as renewable raw material", ChemSusChem **3**, 1227–1235 (2010).

[19] W. Fang, S. Yang, X.-L. Wang, T.-Q. Yuan, and R.-C. Sun, "Manufacture and application of lignin-based carbon fibers (lcfs) and lignin-based carbon nanofibers (lcnfs)", Green Chemistry **19**, 1794–1827 (2017).

[20] E. Svinterikos, I. Zuburtikudis, and M. Al-Marzouqi, "Electrospun lignin-derived carbon micro-and nanofibers: a review on precursors, properties, and applications", ACS Sustainable Chemistry & Engineering **8**, 13868–13893 (2020).

[21] C. Crestini, H. Lange, M. Sette, and D. S. Argyropoulos, "On the structure of softwood kraft lignin", Green Chemistry **19**, 4104–4121 (2017).

[22] A. N. Evdokimov, A. V. Kurzin, O. V. Fedorova, P. V. Lukanin, V. G. Kazakov, and A. D. Trifonova, "Desulfurization of kraft lignin", Wood Science and Technology **52**, 1165–1174 (2018).

[23] S. Hu and Y.-L. Hsieh, "Ultrafine microporous and mesoporous activated carbon fibers from alkali lignin", Journal of Materials Chemistry A **1**, 11279–11288 (2013).

[24] B. A. Deyerle and Y. Zhang, "Effects of hofmeister anions on the aggregation behavior of peo–ppo–peo triblock copolymers", Langmuir **27**, 9203–9210 (2011).

[25] A. Mohamed, "Synthesis, characterization, and applications carbon nanofibers", in *Carbon-based nanofillers and their rubber nanocomposites* (Elsevier, 2019), pp. 243–257.

[26] J. C. Ruiz-Cornejo, D. Sebastián, and M. J. Lázaro, "Synthesis and applications of carbon nanofibers: a review", Reviews in Chemical Engineering **1** (2018).

[27] Y. Xu, Y. Liu, S. Chen, and Y. Ni, "Current overview of carbon fiber: toward green sustainable raw materials", BioResources **15**, 7234–7259 (2020).

[28] G. R. Mitchell, *Electrospinning: principles, practice and possibilities* (Royal Society of Chemistry, 2015).

[29] S. Peng and P. R. Ilango, *Electrospinning of nanofibers for battery applications* (Springer, 2020).

[30] S. Ramakrishna, *An introduction to electrospinning and nanofibers* (World Scientific, 2005).

[31]D. H. Reneker and A. L. Yarin, "Electrospinning jets and polymer nanofibers", Polymer **49**, 2387–2425 (2008).

[32]C. P. Carroll and Y. L. Joo, "Axisymmetric instabilities in electrospinning of highly conducting, viscoelastic polymer solutions", Physics of Fluids **21**, 103101 (2009).

[33]H. Fong, I. Chun, and D. H. Reneker, "Beaded nanofibers formed during electrospinning", Polymer **40**, 4585–4592 (1999).

[34]W. Zuo, M. Zhu, W. Yang, H. Yu, Y. Chen, and Y. Zhang, "Experimental study on relationship between jet instability and formation of beaded fibers during electrospinning", Polymer Engineering & Science **45**, 704–709 (2005).

[35]C. J. Angammana and S. H. Jayaram, "Analysis of the effects of solution conductivity on electrospinning process and fiber morphology", IEEE Transactions on industry applications **47**, 1109–1117 (2011).

[36]T. Uyar and F. Besenbacher, "Electrospinning of uniform polystyrene fibers: the effect of solvent conductivity", Polymer **49**, 5336–5343 (2008).

[37]X. Zong, K. Kim, D. Fang, S. Ran, B. S. Hsiao, and B. Chu, "Structure and process relationship of electrospun bioabsorbable nanofiber membranes", Polymer **43**, 4403–4412 (2002).

[38]D. Fallahi, M. Rafizadeh, N. Mohammadi, and B. Vahidi, "Effects of feed rate and solution conductivity on jet current and fiber diameter in electrospinning of polyacrylonitrile solutions", e-Polymers **9** (2009).

[39]C. Mit-uppatham, M. Nithitanakul, and P. Supaphol, "Ultrafine electrospun polyamide-6 fibers: effect of solution conditions on morphology and average fiber diameter", Macromolecular Chemistry and Physics **205**, 2327–2338 (2004).

[40]T. Jarusuwannapoom, W. Hongrojjanawiwat, S. Jitjaicham, L. Wannatong, M. Nithitanakul, C. Pattamaprom, P. Koombhongse, R. Rangkupan, and P. Supaphol, "Effect of solvents on electro-spinnability of polystyrene solutions and morphological appearance of resulting electrospun polystyrene fibers", European Polymer Journal **41**, 409–421 (2005).

[41]N. Choktaweesap, K. Arayanarakul, D. Aht-Ong, C. Meechaisue, and P. Supaphol, "Electrospun gelatin fibers: effect of solvent system on morphology and fiber diameters", Polymer journal **39**, 622–631 (2007).

[42]W. Liu, C. Huang, and X. Jin, "Electrospinning of grooved polystyrene fibers: effect of solvent systems", Nanoscale research letters **10**, 1–10 (2015).

[43]A. Celebioglu and T. Uyar, "Electrospun porous cellulose acetate fibers from volatile solvent mixture", Materials Letters **65**, 2291–2294 (2011).

[44]G. I. Taylor, "Disintegration of water drops in an electric field", Proceedings of the Royal Society of London. Series A. Mathematical and Physical Sciences **280**, 383–397 (1964).

[45]J. Doshi and D. H. Reneker, "Electrospinning process and applications of electrospun fibers", Journal of electrostatics **35**, 151–160 (1995).

[46]S. Zhao, X. Wu, L. Wang, and Y. Huang, "Electrospinning of ethyl–cyanoethyl cellulose/tetrahydrofuran solutions", Journal of Applied Polymer Science **91**, 242–246 (2004).

[47]C. Zhang, X. Yuan, L. Wu, Y. Han, and J. Sheng, “Study on morphology of electrospun poly (vinyl alcohol) mats”, European polymer journal **41**, 423–432 (2005).

[48]M. M. Demir, I. Yilgor, E. Yilgor, and B. Erman, “Electrospinning of polyurethane fibers”, Polymer **43**, 3303–3309 (2002).

[49]C.-M. Wu, H.-G. Chiou, S.-L. Lin, and J.-M. Lin, “Effects of electrostatic polarity and the types of electrical charging on electrospinning behavior”, Journal of Applied Polymer Science **126**, E89–E97 (2012).

[50]S.-H. Tan, R. Inai, M. Kotaki, and S. Ramakrishna, “Systematic parameter study for ultra-fine fiber fabrication via electrospinning process”, Polymer **46**, 6128–6134 (2005).

[51]L. Kong and G. R. Ziegler, “Quantitative relationship between electrospinning parameters and starch fiber diameter”, Carbohydrate polymers **92**, 1416–1422 (2013).

[52]V. Beachley and X. Wen, “Effect of electrospinning parameters on the nanofiber diameter and length”, Materials Science and Engineering: C **29**, 663–668 (2009).

[53]C. Wang, H.-S. Chien, K.-W. Yan, C.-L. Hung, K.-L. Hung, S.-J. Tsai, and H.-J. Jhang, “Correlation between processing parameters and microstructure of electrospun poly (d, l-lactic acid) nanofibers”, Polymer **50**, 6100–6110 (2009).

[54]S. Zargham, S. Bazgir, A. Tavakoli, A. S. Rashidi, and R. Damerchely, “The effect of flow rate on morphology and deposition area of electrospun nylon 6 nanofiber”, Journal of Engineered Fibers and Fabrics **7**, 155892501200700414 (2012).

[55]H. He, Y. Kara, and K. Molnar, “Effect of needle characteristic on fibrous peo produced by electrospinning”, Resolution and Discovery **4**, 7–11 (2019).

[56]J.-W. Liang, G. Prasad, S.-C. Wang, J.-L. Wu, and S.-G. Lu, “Enhancement of the oil absorption capacity of poly (lactic acid) nano porous fibrous membranes derived via a facile electrospinning method”, Applied Sciences **9**, 1014 (2019).

[57]A. H. Hekmati, A. Rashidi, R. Ghazisaeidi, and J.-Y. Drean, “Effect of needle length, electrospinning distance, and solution concentration on morphological properties of polyamide-6 electrospun nanowebs”, Textile Research Journal **83**, 1452–1466 (2013).

[58]J. Stanger, N. Tucker, A. Wallace, N. Larsen, M. Staiger, and R. Reeves, “The effect of electrode configuration and substrate material on the mass deposition rate of electrospinning”, Journal of applied polymer science **112**, 1729–1737 (2009).

[59]L. Liu and Y. A. Dzenis, “Analysis of the effects of the residual charge and gap size on electrospun nanofiber alignment in a gap method”, Nanotechnology **19**, 355307 (2008).

[60]D. Li, Y. Wang, and Y. Xia, “Electrospinning nanofibers as uniaxially aligned arrays and layer-by-layer stacked films”, Advanced materials **16**, 361–366 (2004).

[61]M. A. A. De Prá, R. M. Ribeiro-do Valle, M Maraschin, and B. Veleirinho, “Effect of collector design on the morphological properties of polycaprolactone electrospun fibers”, Materials Letters **193**, 154–157 (2017).

[62]A. Baji, Y.-W. Mai, S.-C. Wong, M. Abtahi, and P. Chen, “Electrospinning of polymer nanofibers: effects on oriented morphology, structures and tensile properties”, Composites science and technology **70**, 703–718 (2010).

[63]Y. Yang, Z. Jia, Q. Li, and Z. Guan, “Experimental investigation of the governing parameters in the electrospinning of polyethylene oxide solution”, IEEE transactions on dielectrics and electrical insulation **13**, 580–585 (2006).

[64]S. Tripatanasuwan, Z. Zhong, and D. H. Reneker, “Effect of evaporation and solidification of the charged jet in electrospinning of poly (ethylene oxide) aqueous solution”, Polymer **48**, 5742–5746 (2007).

[65]S. De Vrieze, T. Van Camp, A. Nelvig, B. Hagström, P. Westbroek, and K. De Clerck, “The effect of temperature and humidity on electrospinning”, Journal of materials science **44**, 1357–1362 (2009).

[66]C. Wang, H.-S. Chien, C.-H. Hsu, Y.-C. Wang, C.-T. Wang, and H.-A. Lu, “Electrospinning of polyacrylonitrile solutions at elevated temperatures”, Macromolecules **40**, 7973–7983 (2007).

[67]K Sen, P Bajaj, and T. Sreekumar, “Thermal behavior of drawn acrylic fibers”, Journal of Polymer Science Part B: Polymer Physics **41**, 2949–2958 (2003).

[68]I. Dallmeyer, L. T. Lin, Y. Li, F. Ko, and J. F. Kadla, “Preparation and characterization of interconnected, kraft lignin-b ased carbon fibrous materials by electrospinning”, Macromolecular materials and engineering **299**, 540–551 (2014).

[69]G. Wisanrakkit and J. K. Gillham, “Continuous heating transformation (cht) cure diagram of an aromatic amine/epoxy system at constant heating rates”, Journal of applied polymer science **42**, 2453–2463 (1991).

[70]E. I. Akpan, “Stabilization of lignin fibers”, in *Sustainable lignin for carbon fibers: principles, techniques, and applications* (Springer, 2019), pp. 325–352.

[71]Y. Hou, T. Sun, H. Wang, and D. Wu, “Thermal-shrinkage investigation of the chemical reaction during the stabilization of polyacrylonitrile fibers”, Journal of applied polymer science **114**, 3668–3672 (2009).

[72]X. Huang, “Fabrication and properties of carbon fibers”, Materials **2**, 2369–2403 (2009).

[73]J Drbohlav and W. Stevenson, “The oxidative stabilization and carbonization of a synthetic mesophase pitch, part i: the oxidative stabilization process”, Carbon **33**, 693–711 (1995).

[74]J. Braun, K. Holtman, and J. Kadla, “Lignin-based carbon fibers: oxidative thermostabilization of kraft lignin”, Carbon **43**, 385–394 (2005).

[75]I. Brodin, M. Ernstsson, G. Gellerstedt, and E. Sjöholm, “Oxidative stabilisation of kraft lignin for carbon fibre production”, (2012).

[76]Y. Li, D. Cui, Y. Tong, and L. Xu, “Study on structure and thermal stability properties of lignin during thermostabilization and carbonization”, International journal of biological macromolecules **62**, 663–669 (2013).

[77]G. Wu, C. Lu, L. Ling, A. Hao, and F. He, “Influence of tension on the oxidative stabilization process of polyacrylonitrile fibers”, Journal of applied polymer science **96**, 1029–1034 (2005).

[78]M. Yu, C. Wang, Y. Bai, Y. Wang, and B. Zhu, “Evolution of tension during the thermal stabilization of polyacrylonitrile fibers under different parameters”, Journal of applied polymer science **102**, 5500–5506 (2006).

[79]Y. Liu, “Stabilization and carbonization studies of polyacrylonitrile/carbon nanotube composite fibers”, PhD thesis (Georgia Institute of Technology, 2010).

[80]N. Meek, D. Penumadu, O. Hosseinaei, D. Harper, S. Young, and T. Rials, “Synthesis and characterization of lignin carbon fiber and composites”, Composites Science and Technology **137**, 60–68 (2016).

[81]B. A. Newcomb, “Processing, structure, and properties of carbon fibers”, Composites Part A: Applied Science and Manufacturing **91**, 262–282 (2016).

[82]D. Edie, “The effect of processing on the structure and properties of carbon fibers”, Carbon **36**, 345–362 (1998).

[83]M. Lallave, J. Bedia, R. Ruiz-Rosas, J. Rodríguez-Mirasol, T. Cordero, J. C. Otero, M. Marquez, A. Barrero, and I. G. Loscertales, “Filled and hollow carbon nanofibers by coaxial electrospinning of alcell lignin without binder polymers”, Advanced Materials **19**, 4292–4296 (2007).

[84]R Ruiz-Rosas, J Bedia, M Lallave, I. Loscertales, A Barrero, J Rodríguez-Mirasol, and T Cordero, “The production of submicron diameter carbon fibers by the electrospinning of lignin”, Carbon **48**, 696–705 (2010).

[85]V. Poursorkhabi Sharifabad, “Production and evaluation of carbonized electrospun fibers from bioethanol lignin”, PhD thesis (2016).

[86]N Yusof and A. Ismail, “Post spinning and pyrolysis processes of polyacrylonitrile (pan)-based carbon fiber and activated carbon fiber: a review”, Journal of Analytical and Applied Pyrolysis **93**, 1–13 (2012).

[87]E Fitzer, W Frohs, and M Heine, “Optimization of stabilization and carbonization treatment of pan fibres and structural characterization of the resulting carbon fibres”, Carbon **24**, 387–395 (1986).

[88]J Rodríguez-Mirasol, T Cordero, and J. Rodríguez, “High-temperature carbons from kraft lignin”, Carbon **34**, 43–52 (1996).

[89]H. Kleinhans and L. Salmén, “Development of lignin carbon fibers: evaluation of the carbonization process”, Journal of Applied Polymer Science **133** (2016).

[90]R. C. Bansal and M. Goyal, *Activated carbon adsorption* (CRC press, 2005).

[91]T. Burchell, “Carbon fiber composite adsorbent media for low pressure natural gas storage”, Carbon Materials Technology Group, Oak Ridge National Laboratory (2000).

[92]T.-H. Ko, C.-K. Lu, C.-H. Lin, et al., “The effects of activation by carbon dioxide on the mechanical properties and structure of pan-based activated carbon fibers”, Carbon **30**, 647–655 (1992).

[93]P. Carrott, M. R. Carrott, et al., “Lignin–from natural adsorbent to activated carbon: a review”, Bioresource technology **98**, 2301–2312 (2007).

[94]E Gonzalez-Serrano, T Cordero, J Rodriguez-Mirasol, L Cotoruelo, and J. Rodriguez, “Removal of water pollutants with activated carbons prepared from h3po4 activation of lignin from kraft black liquors”, Water research **38**, 3043–3050 (2004).

[95]Y. Zou and B.-X. Han, “High-surface-area activated carbon from chinese coal”, Energy & fuels **15**, 1383–1386 (2001).

[96] M Molina-Sabio, M. Gonzalez, F Rodriguez-Reinoso, and A Sepúlveda-Escribano, "Effect of steam and carbon dioxide activation in the micropore size distribution of activated carbon", Carbon **34**, 505–509 (1996).

[97] P. Schlee, O. Hosseinaei, D. Baker, A. Landmér, P. Tomani, M. J. Mostazo-López, D. Cazorla-Amorós, S. Herou, and M.-M. Titirici, "From waste to wealth: from kraft lignin to free-standing supercapacitors", Carbon **145**, 470–480 (2019).

[98] E. Ra, E Raymundo-Piñero, Y. Lee, and F Béguin, "High power supercapacitors using polyacrylonitrile-based carbon nanofiber paper", Carbon **47**, 2984–2992 (2009).

[99] J. Choma, L. Osuchowski, M. Marszewski, A. Dziura, and M. Jaroniec, "Developing microporosity in kevlar®-derived carbon fibers by co2 activation for co2 adsorption", Journal of CO2 Utilization **16**, 17–22 (2016).

[100] M. A. d. Amaral Junior, J. T. Matsushima, M. C. Rezende, E. S. Gonçalves, J. S. Marcuzzo, and M. R. Baldan, "Production and characterization of activated carbon fiber from textile pan fiber", Journal of Aerospace Technology and Management **9**, 423–430 (2017).

[101] A. M. Puziy, O. I. Poddubnaya, and O. Sevastyanova, "Carbon materials from technical lignins: recent advances", Lignin Chemistry, 95–128 (2020).

[102] H. Wang, Y. Pu, A. Ragauskas, and B. Yang, "From lignin to valuable products–strategies, challenges, and prospects", Bioresource technology **271**, 449–461 (2019).

[103] W. Zhang, J. Yin, Z. Lin, H. Lin, H. Lu, Y. Wang, and W. Huang, "Facile preparation of 3d hierarchical porous carbon from lignin for the anode material in lithium ion battery with high rate performance", Electrochimica Acta **176**, 1136–1142 (2015).

[104] A. Mabrouk, X. Erdocia, M. G. Alriols, and J. Labidi, "Techno-economic evaluation for feasibility of lignin valorisation process for the production of bio-based chemicals", Chemical Engineering Transactions **61**, 427–432 (2017).

[105] K Babeł and K Jurewicz, "Koh activated lignin based nanostructured carbon exhibiting high hydrogen electrosorption", Carbon **46**, 1948–1956 (2008).

[106] S. Hu, S. Zhang, N. Pan, and Y.-L. Hsieh, "High energy density supercapacitors from lignin derived submicron activated carbon fibers in aqueous electrolytes", Journal of Power Sources **270**, 106–112 (2014).

[107] S.-X. Wang, L. Yang, L. P. Stubbs, X. Li, and C. He, "Lignin-derived fused electrospun carbon fibrous mats as high performance anode materials for lithium ion batteries", ACS applied materials & interfaces **5**, 12275–12282 (2013).

[108] J. Jin, B.-j. Yu, Z.-q. Shi, C.-y. Wang, and C.-b. Chong, "Lignin-based electrospun carbon nanofibrous webs as free-standing and binder-free electrodes for sodium ion batteries", Journal of Power Sources **272**, 800–807 (2014).

[109] C. R. Correa, T. Otto, and A. Kruse, "Influence of the biomass components on the pore formation of activated carbon", Biomass and Bioenergy **97**, 53–64 (2017).

[110] K. Fu, Q. Yue, B. Gao, Y. Sun, and L. Zhu, "Preparation, characterization and application of lignin-based activated carbon from black liquor lignin by steam activation", Chemical Engineering Journal **228**, 1074–1082 (2013).

[111]A Kriaa, N Hamdi, and E Srasra, “Adsorption studies of methylene blue dye on tunisian activated lignin”, Russian Journal of Physical Chemistry A **85**, 279–287 (2011).

[112]K Mahmoudi, N Hamdi, A Kriaa, and E Srasra, “Adsorption of methyl orange using activated carbon prepared from lignin by zncl 2 treatment”, Russian Journal of Physical Chemistry A **86**, 1294–1300 (2012).

[113]L. M. Cotoruelo, M. D. Marqués, F. J. Díaz, J. Rodríguez-Mirasol, J. J. Rodríguez, and T. Cordero, “Adsorbent ability of lignin-based activated carbons for the removal of p-nitrophenol from aqueous solutions”, Chemical Engineering Journal **184**, 176–183 (2012).

[114]S. Żółtowska-Aksamitowska, P. Bartczak, J. Zembrzuska, and T. Jesionowski, “Removal of hazardous non-steroidal anti-inflammatory drugs from aqueous solutions by biosorbent based on chitin and lignin”, Science of the Total Environment **612**, 1223–1233 (2018).

[115]M. Asadullah, I. Jahan, M. B. Ahmed, P. Adawiyah, N. H. Malek, and M. S. Rahman, “Preparation of microporous activated carbon and its modification for arsenic removal from water”, Journal of Industrial and Engineering Chemistry **20**, 887–896 (2014).

[116]D. Saha, N. Mirando, and A. Levchenko, “Liquid and vapor phase adsorption of btx in lignin derived activated carbon: equilibrium and kinetics study”, Journal of cleaner production **182**, 372–378 (2018).

[117]O. Santos, M. C. da Silva, V. Silva, W. Mussel, and M. Yoshida, “Polyurethane foam impregnated with lignin as a filler for the removal of crude oil from contaminated water”, Journal of hazardous materials **324**, 406–413 (2017).

[118]J. M. Rosas, R. Ruiz-Rosas, J. Rodríguez-Mirasol, and T. Cordero, “Kinetic study of so2 removal over lignin-based activated carbon”, Chemical Engineering Journal **307**, 707–721 (2017).

[119]Y. Sun, J. P. Zhang, C. Wen, and L. Zhang, “An enhanced approach for biochar preparation using fluidized bed and its application for h2s removal”, Chemical Engineering and Processing: Process Intensification **104**, 1–12 (2016).

[120]G Yang, Y. Sun, C Wen, and J. Zhang, “A fast approach for preparation of adsorbent from reed black liquor and its performance in equilibrium and kinetic gas separation”, Chemical and Biochemical Engineering Quarterly **29**, 375–383 (2015).

[121]Y. Ge and Z. Li, “Application of lignin and its derivatives in adsorption of heavy metal ions in water: a review”, ACS Sustainable Chemistry & Engineering **6**, 7181–7192 (2018).

[122]V. Dodevski, B. Janković, M. Stojmenović, S. Krstić, J. Popović, M. C. Pagnacco, M. Popović, and S. Pašalić, “Plane tree seed biomass used for preparation of activated carbons (ac) derived from pyrolysis. modeling the activation process”, Colloids and Surfaces A: Physicochemical and Engineering Aspects **522**, 83–96 (2017).

[123]M. Kanniche, R. Gros-Bonnivard, P. Jaud, J. Valle-Marcos, J.-M. Amann, and C. Bouallou, “Pre-combustion, post-combustion and oxy-combustion in thermal power plant for co2 capture”, Applied Thermal Engineering **30**, 53–62 (2010).

[124]P. Babu, P. Linga, R. Kumar, and P. Englezos, “A review of the hydrate based gas separation (hbgs) process for carbon dioxide pre-combustion capture”, Energy **85**, 261–279 (2015).

[125]R Ben-Mansour, M. Habib, O. Bamidele, M Basha, N. Qasem, A Peedikakkal, T Laoui, and M. Ali, “Carbon capture by physical adsorption: materials, experimental investigations and numerical modeling and simulations–a review”, Applied Energy **161**, 225–255 (2016).

[126]F. Carrasco-Maldonado, R. Spörl, K. Fleiger, V. Hoenig, J. Maier, and G. Scheffknecht, “Oxy-fuel combustion technology for cement production–state of the art research and technology development”, International Journal of Greenhouse Gas Control **45**, 189–199 (2016).

[127]I. Pfaff and A. Kather, “Comparative thermodynamic analysis and integration issues of ccs steam power plants based on oxy-combustion with cryogenic or membrane based air separation”, Energy Procedia **1**, 495–502 (2009).

[128]L. Zou, Y. Sun, S. Che, X. Yang, X. Wang, M. Bosch, Q. Wang, H. Li, M. Smith, S. Yuan, et al., “Porous organic polymers for post-combustion carbon capture”, Advanced materials **29**, 1700229 (2017).

[129]Z. Zhang, T. N. Borhani, and M. H. El-Naas, “Carbon capture”, in *Exergetic, energetic and environmental dimensions* (Elsevier, 2018), pp. 997–1016.

[130]R. Ahmed, G. Liu, B. Yousaf, Q. Abbas, H. Ullah, and M. U. Ali, “Recent advances in carbon-based renewable adsorbent for selective carbon dioxide capture and separation-a review”, Journal of Cleaner Production **242**, 118409 (2020).

[131]C Hendriks, “Energy conversion: co 2 removal from coal-fired power plant”, Netherlands: Kluwer Academic Publishers (1995).

[132]W. Conway, S. Bruggink, Y. Beyad, W. Luo, I. Melián-Cabrera, G. Puxty, and P. Feron, “Co2 absorption into aqueous amine blended solutions containing monoethanolamine (mea), n, n-dimethylethanolamine (dmea), n, n-diethylethanolamine (deea) and 2-amino-2-methyl-1-propanol (amp) for post-combustion capture processes”, Chemical Engineering Science **126**, 446–454 (2015).

[133]A. Brunetti, F. Scura, G. Barbieri, and E. Drioli, “Membrane technologies for co2 separation”, Journal of Membrane Science **359**, 115–125 (2010).

[134]E. Favre, “Membrane processes and postcombustion carbon dioxide capture: challenges and prospects”, Chemical Engineering Journal **171**, 782–793 (2011).

[135]L. Wang, M. S. Boutilier, P. R. Kidambi, D. Jang, N. G. Hadjiconstantinou, and R. Karnik, “Fundamental transport mechanisms, fabrication and potential applications of nanoporous atomically thin membranes”, Nature nanotechnology **12**, 509 (2017).

[136]D. Y. Leung, G. Caramanna, and M. M. Maroto-Valer, “An overview of current status of carbon dioxide capture and storage technologies”, Renewable and Sustainable Energy Reviews **39**, 426–443 (2014).

[137]A. S. Bhown and B. C. Freeman, “Analysis and status of post-combustion carbon dioxide capture technologies”, Environmental science & technology **45**, 8624–8632 (2011).

[138]S. Krishnamurthy, V. R. Rao, S. Guntuka, P. Sharratt, R. Haghpanah, A. Rajendran, M. Amanullah, I. A. Karimi, and S. Farooq, "Co2 capture from dry flue gas by vacuum swing adsorption: a pilot plant study", AIChE Journal **60**, 1830–1842 (2014).

[139]R. M. Siqueira, G. R. Freitas, H. R. Peixoto, J. F. do Nascimento, A. P. S. Musse, A. E. Torres, D. C. Azevedo, and M. Bastos-Neto, "Carbon dioxide capture by pressure swing adsorption", Energy Procedia **114**, 2182–2192 (2017).

[140]R. T. Maruyama, K. N. Pai, S. G. Subraveti, and A. Rajendran, "Improving the performance of vacuum swing adsorption based co2 capture under reduced recovery requirements", International Journal of Greenhouse Gas Control **93**, 102902 (2020).

[141]L. Joss, M. Gazzani, M. Hefti, D. Marx, and M. Mazzotti, "Temperature swing adsorption for the recovery of the heavy component: an equilibrium-based shortcut model", Industrial & Engineering Chemistry Research **54**, 3027–3038 (2015).

[142]A. Ntiamoah, J. Ling, P. Xiao, P. A. Webley, and Y. Zhai, "Co2 capture by temperature swing adsorption: use of hot co2-rich gas for regeneration", Industrial & Engineering Chemistry Research **55**, 703–713 (2016).

[143]A. Ayoub and R Venditti, "The effect of irradiation on the processability of lignin for carbon fiber applications", in Proceedings of the 2013 aiche annual meeting, hilton san francisco union square, san francisco, ca, usa (2013), pp. 3–8.

[144]H. Yang, R. Yan, H. Chen, D. H. Lee, and C. Zheng, "Characteristics of hemicellulose, cellulose and lignin pyrolysis", Fuel **86**, 1781–1788 (2007).

[145]A. Tejado, C Pena, J Labidi, J. Echeverria, and I Mondragon, "Physico-chemical characterization of lignins from different sources for use in phenol–formaldehyde resin synthesis", Bioresource technology **98**, 1655–1663 (2007).

[146]R. Sun, J. Tomkinson, and G. L. Jones, "Fractional characterization of ash-aq lignin by successive extraction with organic solvents from oil palm efb fibre", Polymer Degradation and Stability **68**, 111–119 (2000).

[147]M. Zhang, F. L. Resende, A. Moutsoglou, and D. E. Raynie, "Pyrolysis of lignin extracted from prairie cordgrass, aspen, and kraft lignin by py-gc/ms and tga/ftir", Journal of Analytical and Applied Pyrolysis **98**, 65–71 (2012).

[148]T. Van de Ven, M. A. Qasaimeh, and J Paris, "Peo-induced flocculation of fines: effects of peo dissolution conditions and shear history", Colloids and Surfaces A: Physicochemical and Engineering Aspects **248**, 151–156 (2004).

[149]M. R. Wu and T. G. van de Ven, "Flocculation and reflocculation: interplay between the adsorption behavior of the components of a dual flocculant", Colloids and Surfaces A: Physicochemical and Engineering Aspects **341**, 40–45 (2009).

[150]A. Goudarzi, L.-T. Lin, and F. K. Ko, "X-ray diffraction analysis of kraft lignins and lignin-derived carbon nanofibers", Journal of Nanotechnology in Engineering and Medicine **5** (2014).

[151]N.-Y. Teng, I. Dallmeyer, and J. F. Kadla, "Incorporation of multiwalled carbon nanotubes into electrospun softwood kraft lignin-based fibers", Journal of Wood Chemistry and Technology **33**, 299–316 (2013).

[152] X. Xu, J. Zhou, L. Jiang, G. Lubineau, S. A. Payne, and D. Gutschmidt, "Lignin-based carbon fibers: carbon nanotube decoration and superior thermal stability", Carbon **80**, 91–102 (2014).

[153] V. Poursorkhabi, A. K. Mohanty, and M. Misra, "Statistical analysis of the effects of carbonization parameters on the structure of carbonized electrospun organosolv lignin fibers", Journal of Applied Polymer Science **133** (2016).

[154] H. Teng, J.-A. Ho, Y.-F. Hsu, and C.-T. Hsieh, "Preparation of activated carbons from bituminous coals with co2 activation. 1. effects of oxygen content in raw coals", Industrial & engineering chemistry research **35**, 4043–4049 (1996).

[155] L. Li, X.-F. Wang, J.-J. Zhong, X. Qian, S.-L. Song, Y.-G. Zhang, and D.-H. Li, "Nitrogen-enriched porous polyacrylonitrile-based carbon fibers for co2 capture", Industrial & Engineering Chemistry Research **57**, 11608–11616 (2018).

# Appendix A

## A.1 Preliminary study

In Table A.1 all the spun solutions in the preliminary study are shown.

Table A.1: Solutions tested in the preliminary study.

| Lignin:PEO | Total polymer content, % | Comments |
|---|---|---|
| 98:2 | 13,3% | Sprays on the collector |
| 95:5 | 11,3% | Multiple jets, too viscous |
| 93:7 | 10,3% | Too viscous to spin |
| 90:10 | 7% | Thick fibres at a very high voltage |
| 85:15 | 7,2% | Beaded fibres at a high voltage |
| 80:20 | 5% | Beaded fibres |
| 93:7 | 10,3% | Too viscous to spin |
| 0:100 | 1% | Spray |
| 0:100 | 1,5% | Spray |
| 0:100 | 2% | Thin fibres |
| 80:20 | 5% | Fibres and spray |
| 33:66 | 2,8% | Fibres and spray |
| 95:5 | 7% | More spray than fibres |
| 95:5 | 5% | Too low viscosity to spin |
| 90:10 | 7% | Thin fibres |
| 95:5 | 10% | Fibres |
| 99:1 | 14,09% | Spray |
| 97:3 | 10% | Too viscous to spin |
| 93:7 | 8,5% | Thin fibres, some spray |

# Appendix B

## B.1 Cyclic $CO_2$ adsorption experiment

The $CO_2$ adsorption-desorption cyclic experiment was carried out using a TA Discovery TGA to precisely measure the mass gain or loss. The flow rate of all gases were 50ml/min. The samples of 2 mg were loaded onto an aluminium pan and initially degassed under an $N_2$ stream at 110°C for 120 min. The temperature was reduced to 25°C at a heating rate of 10°C/min and held for 60 min. Cyclic $CO_2$ adsorption-desorption was analysed by changing the gas to $CO_2$ for 30 min and switched to $N_2$ for 35 min. 10 such cycles were carried out. No desorption of $CO_2$ was seen over the 10 cycles.

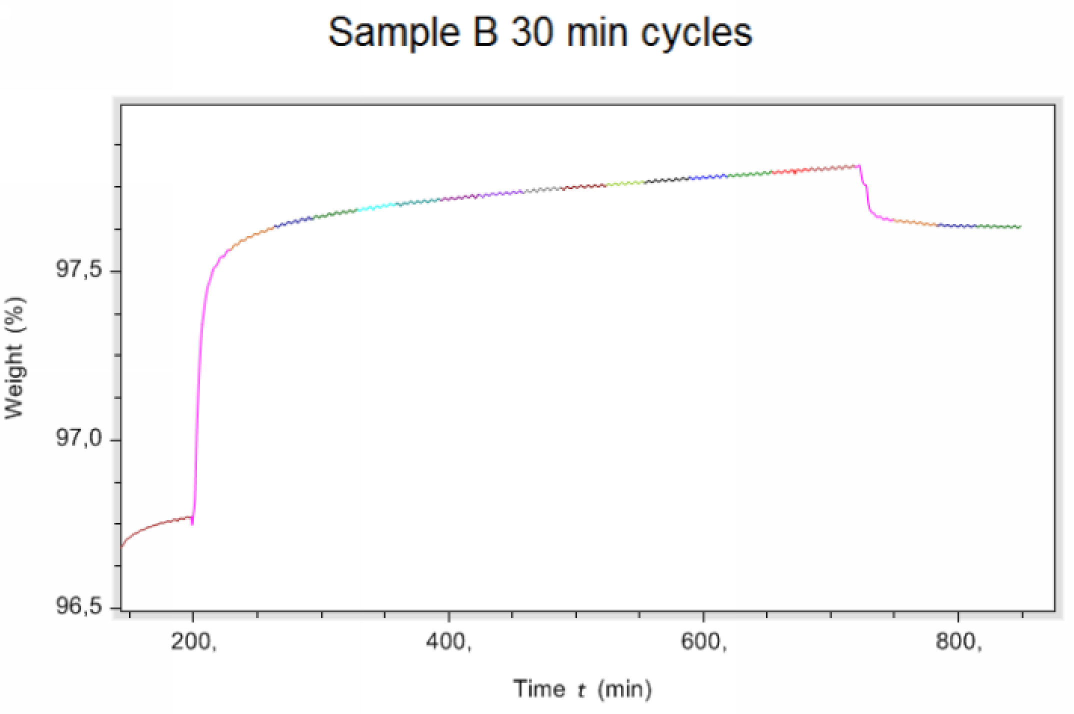

Figure B.1: A cyclic adsorption-desorption of $CO_2$ with 30 minute cycles of adsorption and 35 minutes of desorption